IS-T 1733

Inductively Coupled Plasma Spectrometry: Noise Characteristics of Aerosols, Application of Generalized Standard Additions Method, and Mach Disk as an Emission Source

by

Luan, Shen

PHD Thesis submitted to Iowa State University

Ames Laboratory, U.S. DOE

Iowa State University

Ames, Iowa 50011

Date Transmitted: October 6, 1995

PREPARED FOR THE U.S. DEPARTMENT OF ENERGY

UNDER CONTRACT NO. W-7405-Eng-82.

DISCLAIMER

Inductively coupled plasma spectrometry: Noise characteristics of aerosols, application of generalized standard additions method, and Mach disk as an emission source

Shen Luan

Major Professor: R. S. Houk
Iowa State University

This dissertation is focused on three problem areas in the performance of inductively coupled plasma (ICP) source.

The noise characteristics of aerosols produced by ICP nebulizers are investigated. A laser beam is scattered by aerosol and detected by a photomultiplier tube and the noise amplitude spectrum of the scattered radiation is measured by a spectrum analyzer. Discrete frequency noise in the aerosol generated by a Meinhard nebulizer or a direct injection nebulizer is primarily caused by pulsation in the liquid flow from the pump. By use of a pulse-free pump, the discrete frequency noise is eliminated. The configuration of the spray chamber affects the white noise level. A Scott-type spray chamber suppresses white noise, while a conical, straight-pass spray chamber enhances white noise, relative to the noise seen from the primary aerosol. The noise in the aerosol from a continuous-flow ultrasonic nebulizer has a relatively high 1/f component.

Simultaneous correction for both spectral interferences and matrix effects in ICP atomic emission spectrometry (AES) can be accomplished by using the generalized standard additions method (GSAM). Results obtained with the application of the GSAM to the Perkin-Elmer Optima 3000 ICP atomic emission spectrometer are presented. The

echelle-based polychromator with segmented-array charge-coupled device detectors enables the direct, visual examination of the overlapping lines Cd (I) 228.802 nm and As (I) 228.812 nm. The slit translation capability allows a large number of data points to be sampled, therefore, the advantage of noise averaging is gained. Pure spectra of each of the spectrally active components in the sample can be extracted through the GSAM calculation.

An ICP is extracted into a small quartz vacuum chamber through a sampling orifice in a water-cooled copper plate. Optical emission from the Mach disk region is measured with a new type of echelle spectrometer equipped with two segmented-array charge-coupled-device detectors, with an effort to improve the detection limits for simultaneous multielement analysis by ICP-AES. The analyte line intensities are enhanced at higher pressure in the expansion chamber.

TABLE OF CONTENTS

CHAPTER 1. GENERAL INTRODUCTION

The inductively coupled plasma (ICP) was first studied as an optical emission source in the early 1960s (1-3). Since that time, the ICP has become the dominant source for atomic emission spectrometry (AES). The ICP-AES technique is perhaps by far the most common technique for routine multi-element analysis, as evidenced by the fact that there are roughly 15,000 such instruments in routine use throughout the world, and each day at least 1,000,000 analytical determinations are done by this technique. Unofficial estimates of the current market in ICP-AES systems place total sales at 1,000 instruments per year. About 16 manufacturers worldwide offer more than 30 different types of ICP-AES systems (4).

Another major breakthrough in the field of ICP took place in 1980 (5), when the ICP was shown to be an excellent ionization source for mass spectrometry (MS). In just about 15 years, the ICP-MS technique has already exerted a phenomenal impact on analytical atomic spectrometry. ICP-MS offers part per trillion detection limits (which are often 3 orders of magnitude superior to those in ICP-AES), simple isotopic analysis capability (without the complexity of resolving the isotopic lines in ICP-AES), and virtually complete elemental coverage across the periodic table (6). ICP-MS is regarded as "a multi-elemental analysis technique with almost unlimited potential" (7). It is estimated that at the time of writing the number of ICP-MS instruments worldwide is roughly 1,000, despite the relatively high cost and the young age of ICP-MS. There are about 12 ICP-MS manufacturers worldwide.

In this general introduction, the characteristics of the ICP which lead to its successful analytical virtues will be briefly reviewed. The remaining problem areas of ICP techniques will be briefly assessed, which lead to the research of this dissertation.

Operation of the ICP

A plasma, by definition, is a hot, partially ionized gas. The ICP is generated and sustained in the plasma torch, as illustrated in Figure 1. The main body of the plasma torch consists of an assembly of concentric quartz tubes surrounded by a load coil that is connected to a radio-frequency (RF) generator. The load coil is a few turns of copper tube cooled by a water flow. The RF generator is operated at either 27 or 40 megahertz (MHz). Typically, the RF output power is 500 to 2000 watts. An inert gas, usually argon, is supplied to the plasma torch in several separate flows. The outer gas (usually 10 to 20 l min^{-1}) is injected tangentially and spirals from the annular space between the outer and middle tubes. This flow of gas acts as the support gas for the plasma and also as the coolant gas for the outer quartz tube. To initiate the plasma, a spark from a Tesla coil or an ignitor is used to produce "seed" electrons. These electrons then interact with the time-varying magnetic field induced by the RF current flowing through the load coil at the frequency of the generator and precess around the magnetic field lines in closed, circular orbits. Thus, the electrical energy supplied to the load coil is converted into the kinetic energy of electrons. Adding energy to the electrons by the use of a load coil in this manner is known as *inductive coupling*. Because the plasma is at atmospheric pressure, the mean free path is very short (about 10^{-5} cm) and the electrons

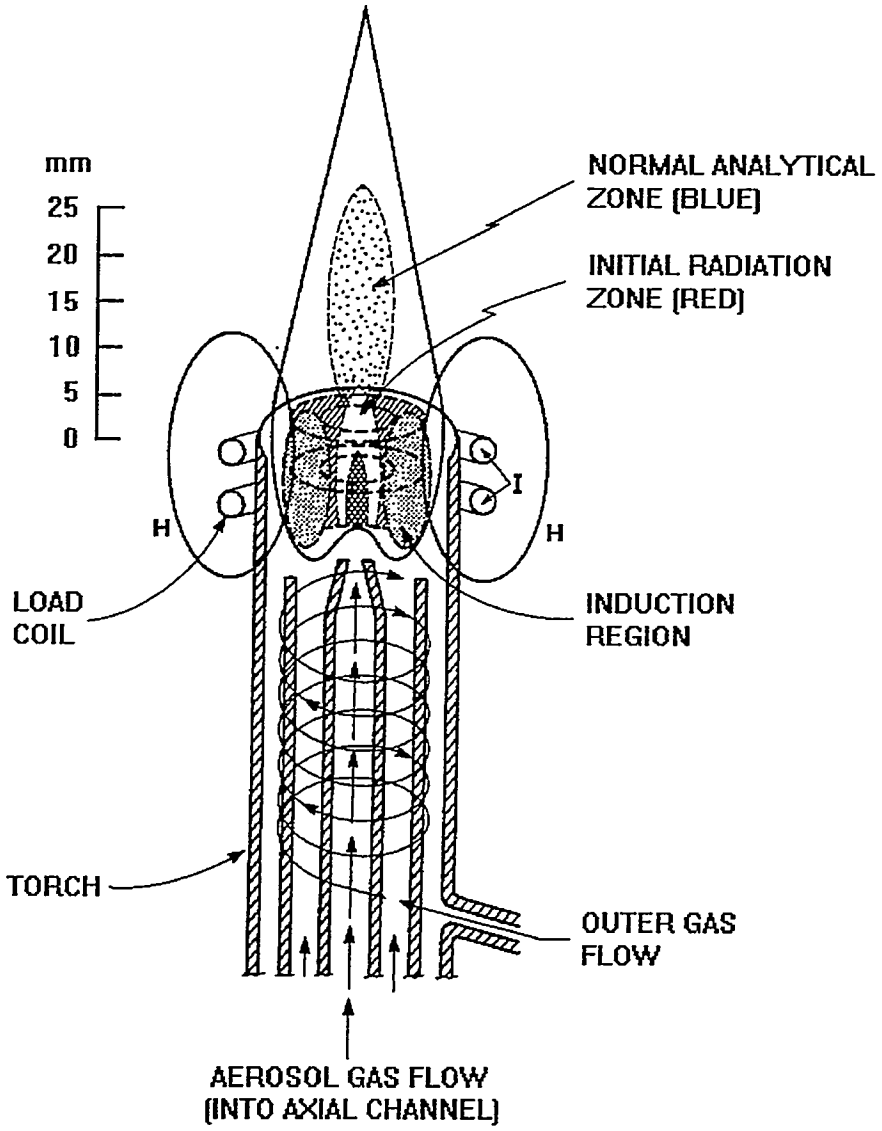

Figure 1. Schematic diagram of ICP, torch, gas flows, and the induced magnetic field. The shaded zones are observed when a nebulized sample containing Y is introducd via the aerosol gas flow. Reproduced with permission from Reference 8.

collide frequently with neutral argon atoms. These collisions sustain the ionization and heat the gas, causing formation of an extended, stable plasma, known as an ICP.

The ICP appears as a very intense, brilliant white, teardrop-shaped discharge. At the frequencies used, the skin-depth effect occurring in RF induction heating ensures that most of the energy is coupled into the outer region of the plasma. This zone is often called the induction region for this reason. The intermediate gas flow (usually 0 to 1.5 l min^{-1}) which is introduced to the inner annular space, termed the auxiliary flow, is mainly used to ensure that the hot plasma is kept clear of the tip of the central injector tube, to prevent its being melted. The central gas flow, often called injector, nebulizer, or carrier gas flow, conveys the sample from the sample introduction system, and is usually around 1 l min^{-1}. At the base of the ICP, the plasma is toroidal, or doughnut-shaped because the nebulizer flow literally punches a cooler hole through the center of the ICP. This region is often called the central or axial channel. The axial channel is enclosed and heated by the induction region. Note that the RF power is coupled into the plasma in a region that is physically distinct from that where the sample is located. Thus, the composition of the sample can change over a substantial range without perturbing the basic electrical processes that sustain the plasma. The confinement of the analytes in the axial channel greatly facilitates the collection of photons and ions for analytical purposes (8-16).

Conditions in the Axial Channel

The axial channel is the area where the sample is introduced and mixed with hot plasma originating from the torodial induction region. Gas kinetic temperatures in the axial channel reach approximately 5,000 K to 6,000 K at the mouth of the torch. Additionally, the sample residence time in the axial channel is about 4 ms. The combination allows adequate transfer of energy to the analytes to convert them into free atoms and ions for analysis.

Solutions are by far the most common form of samples. A nebulizer converts sample solution into a mist of fine droplets, called an aerosol. The droplets are then injected into the ICP along the axial channel. The following reactions represent the processes that take place when an aerosol is introduced into an ICP.

Desolvation: $MX\ (wet\ droplet) \rightarrow MX\ (dry\ particle)$ . . . . . (1)

Vaporization: $MX\ (dry\ particle) \rightarrow MX\ (g)$ . . . . . (2)

Atomization: $MX\ (g) \rightarrow M\ (g) + X\ (g)$ . . . . . (3)

Ionization: $M \rightarrow M^+ + e^-$ . . . . . (4)

Excitation: $M \rightarrow M^* \rightarrow M + h\upsilon$ . . . . . (5)

$M^+ \rightarrow (M^+)^* \rightarrow M^+ + h\upsilon'$ . . . . . (6)

Here the asterisks denote excited electronic states of the ions or neutral atoms.

Some of these processes can readily be observed to occur in the axial channel of the ICP when a concentrated solution of yttrium is introduced (Figure 1). The initial radiation zone (IRZ) low in the ICP appears as a hollow, bullet-shaped region of intense red emission, which corresponds to emission from both excited Y atoms and YO

molecules. The plasma region of the greatest analytical utility, the normal analytical zone (NAZ), is above the IRZ. In the NAZ, ionization becomes much more extensive. The strong blue emission from singly charged, positive Y ions predominates in the NAZ. It has been shown that most elements of the periodic table are highly ionized (>90%) in the NAZ. Although production of singly charged ions is very efficient in the ICP, ionization conditions are not very energetic, and the temperature and electron number density are such that relatively few doubly charged ions are formed (8, 9, 11, 12, 15-18).

Attributes and Problems of the ICP Source

The advantages and remaining problems (6, 7, 13, 19-21) related to the use of ICP source for AES and MS are compiled in Table 1. Apparently, efficient approaches to deal with these problems will greatly expand the capabilities of ICP techniques.

Dissertation Objectives and Organization

This dissertation is focused on three problem areas in the performance of ICP source, including:

1. Characterization of noise introduced by the sample introduction system;
2. Simultaneous correction for both spectral interferences and matrix effects in ICP-AES;
3. Measurement of line emission from analyte atoms and ions without the high continuum background, with an attempt to improve the detection limits of ICP-AES.

Table 1. Attributes and problems related to the use of ICP source for AES and MS

Attributes:	Low detection limits
	Multielement analysis (simultaneous or rapid sequential)
	Wide linear dynamic range
Problems:	Spectral interferences
	Matrix effects
	Limited precision and drift
	Inefficient sample introduction
	Difficulty in analyzing solid samples without dissolution
	Detection limits not low enough for some applications

Chapter 2, Chapter 3, and Chapter 4 of this dissertation are presented such that each chapter stands alone as a complete scientific manuscript with accompanying references, tables, and figures. Each chapter is a paper either published in or submitted to a research journal. Chapter 5 of this dissertation is a general conclusion chapter.

Chapter 2 aims at the precision issue of the ICP techniques. In ICP spectrometry, the precision that can be achieved is often believed to be limited by the sample introduction system (22, 23). To improve the stability and the precision of the ICP sample introduction system, the sources of noise should be isolated and characterized. Despite the numerous studies of noise behavior of mass spectrometric or emission signals

from the ICP, no other published results characterize the noise behaviour of the aerosols themselves in a thorough manner. This is the objective of this chapter.

Chapter 3 is focused on the correction for spectral interferences and matrix effects in ICP-AES. The generalized standard additions method (GSAM) (24) is a multivariate extension of the conventional standard additions method for simultaneous multicomponent determinations. The GSAM looks promising as a method by which both spectral interferences and matrix effects can be overcome simultaneously. The GSAM has been applied to ICP direct-reading polychromators for simultaneous correction for spectral interferences and matrix effects (25). The biggest development in recent years has been the use of charge-transfer devices (CTDs), either charge-coupled devices (CCDs) or charge-injection devices (CIDs), as two-dimensional (2-D) array detectors for ICP-AES (4). The CTD-based instruments, which take advantage of echelle gratings for 2-D spectral dispersion, are true simultaneous detectors. In contrast to the direct-reading spectrometer, they collect emitted light in all of the wavelength ranges monitored at the same time. They also expand the number of wavelengths to hundreds or even thousands of lines, which can be a great advantage over a polychromator with fixed exit slit/photomultiplier tube detector systems. The echelle grating optical system with 2-D array detector offers a convenient way to implement spectral scans for GSAM. In this chapter, a case study of how the GSAM can be applied to an echelle-base spectrometer with two segmented-array charge-coupled device detectors (SCDs) (26) is presented.

Chapter 4 intends to improve the detection limits for simultaneous multielement analysis by ICP-AES. With the recent development of SCD-based ICP optical

spectrometer, the analytical detection limits were shown to be only limited by the photon shot noise of the ICP spectral background (26, 27). One way to improve the detection limits is to reduce the spectral background. The spectral background emitted by the reduced-pressure plasma extracted from an atmospheric pressure ICP was demonstrated to be so low that it was indistinguishable from the dark current of the photomultiplier used (28). The main objective of this chapter is to evaluate the joint use of the reduced-pressure plasma emission source extracted from an ICP with an echelle-based spectrometer equipped with SCDs.

References

1. Wendt, R. H., and Fassel, V. A., *Anal. Chem.*, 1965, **37**, 920.
2. Fassel, V. A., and Kniseley, K. N., *Anal. Chem.*, 1974, **46**, 1110A and 1115A.
3. Greenfield, S., Jones, J. L., and Berry, C. T., *Analyst*, 1964, **89**, 713.
4. Noble, D., *Anal. Chem.*, 1994, **66**, 105A.
5. Houk, R. S., Fassel, V. A., Flesch, G. D., Svec, H. J., Gray, A. L., and Taylor, C. E., *Anal. Chem.*, 1980, **52**, 2283.
6. Hieftje, G. M., Galley, P. J., Glick, M., and Hanselman, D. S., *J. Anal. At. Spectrom.*, 1992, **7**, 69.
7. Beauchemin, D., *Trends Anal. Chem.*, 1991, **10**, 71.
8. Houk, R. S., in *Handbook of the Physics and Chemistry of Rare Earths*, eds. Gschneidner, K. A., Jr., and Eyring, L., Elsevier, New York, 1990, vol. 13, ch. 89.

9. Jarvis, K. E., Gray, A. L., and Houk, R. S., *Handbook of Inductively Coupled Plasma Mass Spectrometry*, Blackie & Son, Glasgow, 1992.

10. Fassel, V. A., *Science*, 1978, **202**, 183.

11. Barnes, R. M., *CRC Crit. Rev. Anal. Chem.*, 1978, **7**, 203.

12. *Inductively Coupled Plasma in Analytical Atomic Spectrometry*, 2nd ed., eds. Montaser, A., and Golightly, D. W., VCH Publishers, New York, 1992.

13. Olesik, J. W., *Anal. Chem.*, 1991, **63**, 12A.

14. Meyer, G. A., *Anal. Chem.*, 1987, **59**, 1345A.

15. Blades, M. W., and Weir, D. G., *Spectroscopy*, 1994, **9**(8), 14.

16. Ingle, J. D., Jr., and Crouch, S. R., *Spectrochemical Analysis*, Prentice Hall, Englewood Cliffs, New Jersey, 1988.

17. Koirtyohann, S. R., Jones, J. S., and Yates, D. A., *Anal. Chem.*, 1980, **52**, 1966.

18. Houk, R. S., *Anal. Chem.*, 1986, **58**, 97A.

19. Hieftje, G. M., *J. Anal. At. Spectrom.*, 1992, **7**, 783.

20. Beauchemin, D., *Spectroscopy*, 1992, **7**(7), 12.

21. Houk, R. S., *Acc. Chem. Res.*, 1994, **27**, 333.

22. Browner, R. F., and Boorn, A. W., *Anal. Chem.*, 1984, **56**, 786A and 875A.

23. Sneddon, J., in *Sample Introduction in Atomic Spectrometry*, ed. Sneddon, J., Elsevier, Amsterdam, 1990, ch. 1, p. 1.

24. Saxberg, B. E. H., and Kowalski, B. R., *Anal. Chem.*, 1979, **51**, 1031.

25. Kalivas, J. H., and Kowalski, B. R., *Anal. Chem.*, 1981, **53**, 2207.

26. Barnard, T. W., Crockett, M. I., Ivaldi, J. C., Lundberg, P. L., Yates, D. A., Levine, P. A., and Sauer, D. J., *Anal. Chem.*, 1993, **65**, 1231.

27. Ivaldi, J. C., and Barnard, T. W., *Spectrochim. Acta, Part B*, 1993, **48**, 1265.

28. Houk, R. S., and Lim, H. B., *Anal. Chem.*, 1986, **58**, 3244.

CHAPTER 2. NOISE CHARACTERISTICS OF AEROSOLS PRODUCED BY INDUCTIVELY COUPLED PLASMA NEBULIZERS[1]

A paper published in the Journal of Analytical Atomic Spectrometry[2]

Shen Luan, Ho-ming Pang, Sam C. K. Shum, and R. S. Houk[3]

Abstract

The noise characteristics of aerosols produced by inductively coupled plasma nebulizers were investigated. A laser beam was scattered by aerosol and detected by a photomultiplier tube and the noise amplitude spectrum of the scattered radiation was measured by a spectrum analyzer. Discrete frequency noise in the aerosol generated by a Meinhard nebulizer or a direct injection nebulizer was primarily caused by pulsation in the liquid flow from the pump. By use of a pulse-free pump, such as a gas displacement pump or a dual piston pump for liquid chromatography, the discrete frequency noise was eliminated. The configuration of the spray chamber affected the white noise level. A Scott-type spray chamber suppressed white noise, while a conical, straight-pass spray chamber enhanced white noise, relative to the noise seen from the primary aerosol. The

---

[1] Presented at the 1992 Winter Conference on Plasma Spectrochemistry, San Diego, CA, USA, January 6-11, 1992.

[2] *J. Anal. At. Spectrom.*, 1992, **7**, 799-805.

[3] To whom correspondence should be addressed.

noise in the aerosol from a continuous-flow ultrasonic nebulizer had a relatively high 1/f component.

Keywords: *Noise amplitude spectra; aerosols; nebulizers; inductively coupled plasma mass spectrometry; inductively coupled plasma atomic emission spectrometry*

Introduction

The precision, detection limits, and dynamic range of instrumental measurements, including inductively coupled plasma mass spectrometry (ICP-MS) and inductively coupled plasma atomic emission spectrometry (ICP-AES), are generally influenced by noise in the measured signals. The optimization of experimental variables is often based on reducing the relative amount of noise or increasing the signal-to-noise ratio (S/N). However, the S/N provides only an inclusive view of system performance. A more fundamental understanding of noise characteristics requires a knowledge of the noise power spectrum (NPS), which may identify the types, origins, and frequency composition of the noise. Information on noise characteristics sometimes provides a sound rationale for improving the performance of the instrument.

The NPS for ICP-MS (1-3) and ICP-AES (4-15) have been reported and the prevailing noise types identified as: (*i*) white noise, (*ii*) 1/f noise, and (*iii*) interference noise (16). Noise in the ICP from large, undesolvated wet droplets and undissociated dry particles has also been characterized extensively (17-22). In ICP spectrometry, the precision achievable is often believed to be limited by the sample introduction

system (23-26). To improve the stability and the precision of the ICP sample introduction system, the sources of noise should be isolated and characterized. Despite the numerous studies of noise behavior of mass spectrometric or emission signals from the ICP, we know of no published results that characterize the noise behavior of the aerosols themselves in a thorough manner. This is the objective of the present work. Montaser and co-workers have described interferometric measurements of light scattered from aerosols produced by ultrasonic nebulizers (27). These results have not yet been published, and the main objective of Montaser's study was to measure droplet sizes and velocities rather than noise behavior.

Experimental

Fig. 1 gives a block diagram of the experimental setup used for noise measurements. Table 1 summarizes the instrumentation used. The experiments were performed in a darkened room. Vibrations and air flows were minimized.

The spectrum analyzer actually displayed the square root of the power spectrum, sometimes called the amplitude spectrum. The ordinate of all plots was scaled in units of dBV [1 dBV = 20 log A, where A was the signal amplitude in volts root mean square (RMS)]. Note that this dBV unit was essentially an absolute measure of the noise level, whereas the dB unit in our previous work (1) measured noise (at a specific frequency) relative to the d.c. level. The spectra shown below were not normalized to the d.c. level, so that the d.c. level (*i.e.*, the scattering signal) observed for the various nebulizers and spray chambers could also be presented. Since the dBV scale is

logarithmic, the reader can readily convert from dBV to relative units (*i.e.*, dB) by simply taking the difference between the noise amplitude at the frequency of interest and the dBV reading at the d.c. level (frequency = 0 Hz).

The apparatus shown in Fig. 1 was similar to that used for laser doppler spectroscopy (LDS) for particle size measurements (36). In the present work, aerosol droplet size was not measured. Instead, noise amplitude spectra (NAS) were taken to characterize the noise sources in the aerosols generated by ICP nebulizers. The noise behavior of the laser light scattered from the aerosol droplets was assumed to be related to noise processes in the production and transport of the aerosol itself. Spectra measured at several scattering angles had the same basic features as those measured at 15°, which was used subsequently because it provided the highest scattering signal.

A Meinhard nebulizer (Table 1) was studied because of its common use in ICP spectrometry. Distilled, deionized water was the only sample used in this work. Different pumps were employed to deliver water to the Meinhard nebulizer, as shown in Table 1. Self-priming aspiration (or natural uptake) was also investigated.

The direct injection nebulizer (DIN) was similar to those described (29-33). The i.d. of the sample capillary was 30 μm (33). A single head liquid chromatography (LC) pump (Table 1), a dual head LC pump (Table 1), and a home-made gas displacement pump (29) were used to deliver water to the DIN.

Aerosol NAS were measured directly on the aerosol from the Meinhard nebulizer or DIN and after the primary aerosol passed through either a Scott-type, double-pass spray chamber or a conical, straight-pass spray chamber (Table 1). Ideally, the tertiary

aerosol should also be probed at the exit port of the injector tube of ICP torch (37, 38). This was not feasible, however, because the wet aerosol condensed at the cold tip of the injector tube (38).

The aerosol that coalesced on the inside surface of the spray chamber eventually flowed to the chamber drain and then to a waste receptacle. Irregularities in this flow may have caused pressure fluctuations in the chamber as the liquid flow ran into the waste receptacle. In the present work, appropriate steps were taken to suppress these pressure pulsations (35, 39-43).

Finally, noise in the aerosol generated with an ultrasonic nebulizer (USN) was studied (Table 1). Water was introduced into the USN using the dual head LC pump (Table 1). Again, NAS were measured on the wet droplets leaving a straight-pass spray chamber. Desolvation was not employed. The spatial position where the aerosol was produced on the transducer face plate fluctuated with time, which precluded reliable measurements of NAS of the primary aerosol issuing directly from the surface of the USN.

Argon was used throughout the present work as nebulizer gas (for the pneumatic nebulizers) and carrier gas (for the USN). The flow rate was controlled with a Matheson 7600 series flowmeter equipped with tube no. 602 (Matheson Gas Products, Secaucus, NJ). The needle valve on this flowmeter was positioned at the outlet. This arrangement allowed accurate measurements of flow rate for any back-pressure (or downstream pressure) provided that the gas pressure fed to the flowmeter stayed equal to the pressure for which the tube was calibrated.

Each nebulization system was oriented horizontally on a movable platform such that the distance between the nebulizer tip or the outlet of the spray chamber and the point of interaction with the laser beam could be altered. Usually, the distance was 10.0 mm. The vertical position was also adjusted so that the laser beam could be directed into the center of the aerosol plume.

Results and Discussion

Control Experiments

A series of experiments were performed without nebulizers to determine if the measurement system (*i.e.*, laser, PMT, and spectrum analyzer) contributed any significant noise. NAS were measured from (*i*) the d.c. current output of a battery, connected directly to the input of the spectrum analyzer, (*ii*) the output of a flashlight directed onto the PMT, (*iii*) the attenuated output of the laser, sent directly onto the PMT, and (*iv*) laser scattering from a piece of abrasive paper with 42 μm diameter particles, detected by the PMT. In each case the signal measured by the picoammeter was $\approx$ 1 μA, which was similar to the magnitude of the scattering signal seen subsequently from aerosols. For each control experiment, the white noise was less than -120 dBV. Some small discrete frequency peaks ($<$ -110 dBV) were also observed. All these "instrumental" noise levels were insignificant compared to the noise levels in the light scattered from the aerosols. Furthermore, the background current of the PMT was $\approx$ 3 pA, which was also insignificant compared to the usual scattering signals

of $\approx$ 1 μA. Based on these results, the apparatus did not contribute appreciable noise compared to that seen from the light scattered by the aerosols.

Noise from Aerosol Generated by Meinhard Nebulizer

Fig. 2(*a*) shows the NAS of scattering from the aerosol generated by a Meinhard nebulizer with liquid delivered by a peristaltic pump. Three types of noise are observed: white noise (*i.e.*, the asymptote at the higher end of the frequency axis), 1/f noise (the gradual decline of noise amplitude as frequency increases from 0 Hz), and interference noise (the peaks at discrete frequencies). The frequency axis in Fig. 2(*a*) stopped at 10 Hz because no discrete noise peaks were seen at higher frequencies, which was the case for all the nebulizers, pumps, etc. evaluated in this study.

In Fig. 2(*a*), the interference noise peaks at 1.88 and 2.84 Hz were harmonics of the 0.96 Hz fundamental noise. The frequencies of these peaks did not change as the nebulizer gas flow rate and the distance between the nebulizer tip and the point of interaction with the laser beam (*i.e.*, the "scattering position") were changed. However, the peak frequencies increased with liquid flow rate (Table 2). At each liquid flow rate studied, the fundamental frequency of the pulsation measured from the NAS was essentially the same as the frequency with which a fresh roller touched the compressible pump tubing as the head of the pump rotated. Thus, the pulsation in the liquid flow induced the discrete noise peaks observed in the NAS. Similar peaks have been seen in NPS from ICP signals (2, 3, 14).

Also, similar peaks at discrete frequencies were seen from NAS taken when the Meinhard nebulizer was fed by the syringe pump or the single head LC pump (Table 3). In each case, the frequency of the fundamental noise peak was the same as the frequency of a fluctuation in the liquid flow rate caused by the mechanism that drove the pump (44-46). The amplitude of these noise peaks was lowest ($\approx$ -30 dBV) for the syringe pump, but such peaks were still present, which rebutted the occasional claim that syringe pumps deliver pulseless flow. The dual head LC pump (46, 47) did not produce detectable interference noise peaks.

As shown in Fig. 2(*a*), harmonic peaks were seen at both odd and even integer multiples of the fundamental frequency. The intensity of the harmonic peaks fell off as frequency increased. A similar pattern of harmonic peaks is obtained in the frequency domain when a full-wave rectified sine wave in the time domain is subjected to the Fourier transform process (48). Thus, the liquid flow from the peristaltic pump, the syringe pump, and the single head LC pump is modulated by a full-wave rectified sine wave pattern, which is physically reasonable. Fourier transformation of a sawtooth wave also yields this pattern of harmonics in the frequency domain, but the flow output of a pump probably does not have a sawtooth character.

Self-priming aspiration (or natural uptake) was also used to deliver liquid. As expected, no discrete frequency peaks were present in the noise spectra [Fig. 2(*b*)]. Comparison of Figs. 2(*a*) and 2(*b*) showed that the white noise level (*i.e.*, the baseline asymptote at high frequency) was higher by about 10 dBV when the Meinhard nebulizer was fed by natural uptake, for unknown reasons.

Noise from Aerosol Generated by DIN

Fig. 3 shows the NAS from a DIN aerosol using a single head LC pump. Without the pulse damper, substantial interference noise was observed [Fig. 3(*a*)]. The frequency of the fundamental noise was found to be 0.020 Hz, which again corresponded to the frequency of the pumping/refill stroke at the low liquid flow rate used (50 μL min^{-1}). With the pulse damper, the interference noise was eliminated [Fig. 3(*b*)].

Pulse-free pumps, including a dual head LC pump (with pulse damper) and a gas displacement pump (29), were investigated with the DIN. As expected, no interference noise was present. Only the pulse-free pumps were used for subsequent experiments to suppress noise peaks so that the 1/f structure in the NAS could be seen clearly.

It is interesting that the NAS obtained with a single head LC pump (with pulse damper), a dual head LC pump (with pulse damper), and a gas displacement pump, all gave basically identical 1/f profiles and similar white noise levels (measured relative to the d.c. level). Thus, the white noise and 1/f noise in the NAS were not greatly influenced by the pumps used.

Comparison of Noise from Meinhard Nebulizer and DIN

Fig. 4 compares the NAS of scattering from the aerosol from the Meinhard nebulizer to that from the DIN. These two spectra would be quite similar if they were normalized to the same d.c. level. In each case, the white noise levels were $\approx$ 50 dBV below the d.c. level. The d.c. levels were related to the total scattering signals seen from

the two nebulizers. These d.c. levels differed by $\approx$ 15 dBV because the liquid flow rates and droplet size distributions were different for the two nebulizers.

The contribution of white noise to the RSD of a measured signal can be estimated from the white noise level N (in dB) using the following equation (1, 10):

$$RSD \approx 10^{N/20} \quad \ldots\ldots\ldots\ldots\ldots\ldots\ldots\ldots\ldots\ldots\ldots\ldots \quad (i)$$

The value of N is measured below (or relative to) the d.c. level. For example, in Fig. 4, B the white noise level is -65 dBV and the d.c. level is -15 dBV, so N in equation (i) is (-65) - (-15) = -50 dB. This subtraction process is equivalent to normalizing the noise amplitude at the chosen frequency to the d.c. level.

In the present study, white noise levels of $\approx$ -48 to -50 dB were observed for both the Meinhard nebulizer and the DIN. Thus, white noise as the sole noise source would be expected to yield relative standard deviations (RSDs) of 0.3 - 0.4 %. These RSDs were comparable to those obtained from DIN experiments in ICP-MS at relatively high signal levels ($\approx 10^5$ - 10^6 counts s^{-1}) (29). In contrast, this level of white noise is a minor contribution to the total signal instability of $\approx$ 2 % RSD or worse that is typical of many different ICP-MS devices at high signal levels when a Meinhard nebulizer is used (49).

Effect of Spray Chamber on Noise from Aerosol

Fig. 5 shows the NAS from aerosol from a Meinhard nebulizer after it passed through a Scott-type, double-pass spray chamber with the use of a relatively pulseless pump (the dual head LC pump). No discrete frequency noise was observed. Note that the

white noise level N was ≈ (-82) - (-22) = -60 dB (Fig. 5), which was ≈ 10 dB lower than that present in the primary aerosol (Fig. 4, A). The -60 dB value would correspond to an RSD of ≈ 0.1 %. Compared to the RSDs of 0.3 - 0.4 % expected for the primary aerosol (as described in the proceeding paragraph), the Scott-type, double pass spray chamber apparently improved precision by a factor of 3 to 4.

Fig. 6 shows the NAS from aerosols that were passed through a conical, straight-pass spray chamber. Again, no discrete peaks were observed. Apparently, neither spray chamber contributed noticeable interference noise. Thus, the usual audible noise peaks at 200 - 400 Hz that were seen in either ICP-MS or ICP-AES (10, 15) can not be blamed on either the nebulizer or the spray chamber.

Without argon make-up gas flow (introduced through the spray chamber), the 1/f noise in Fig. 6, A was very large as indicated by the slow decline in noise amplitude as frequency increased. Next, an argon make-up gas was added through the drain tube of the spray chamber (35) at 0.5 L min^{-1}. The total gas flow rate (*i.e.*, the nebulizer gas flow rate plus the make-up gas flow rate) was 1.5 L min^{-1}. Addition of the make-up gas suppressed the 1/f noise substantially (Fig. 6, B). Thus, the gas flow patterns through a spray chamber can affect the characteristics of noise in the aerosol leaving the chamber. Also, it is interesting to note that the white noise level N in Fig. 6, B is ≈ (-43) - (-8) = -35 dB, which is ≈ 15 dB higher than that present in the primary aerosol (Fig. 4, A). This indicated that the precision was poorer (by a factor of 5 to 6) after the aerosol passed through the conical, straight-pass spray chamber. This degradation in precision agreed with previous experience with the use of a conical,

straight-pass spray chamber in ICP-MS experiments with the DIN (29) and in other experience in ICP-AES (50).

The effect of the two spray chambers on 1/f noise was illustrated by comparing the NAS from the primary aerosol produced by the Meinhard nebulizer with the NAS from the secondary aerosol produced by the same Meinhard nebulizer after passage through either a Scott-type, double pass spray chamber or a conical, straight-pass spray chamber. In this case only, each of these spectra were normalized to the same white noise level (-1.0). As shown in Fig. 7, this normalization process facilitated visual comparison of the extent to which noise amplitude dropped off as frequency increased. Curves B and C were obtained with spray chambers. The 1/f portions of these two curves were similar and laid slightly below that for curve A. In other words, the noise dropped off somewhat faster and approached the white noise limit at a lower frequency when either spray chamber was used. Thus, use of either spray chamber apparently attenuated 1/f noise slightly. Such information was hard to discern unless the spectra were normalized to the same white noise level.

Noise from Aerosol Generated by USN

Fig. 8 shows the NAS of the aerosol generated by an USN with the usual straight-pass spray chamber (35). The d.c. signal (*i.e.*, the point at 0 Hz) was 13 dBV higher than that for the Meinhard nebulizer at a comparable total gas flow rate (1.5 L min^{-1}, Fig. 6, B). A higher scattering signal was expected from the USN, partly because of its higher uptake rate (2.5 mL min^{-1}). Fig. 8 also showed that, a fairly large amount of 1/f

noise was observed from the USN. The noise amplitude still dropped as frequency increased out to frequencies of at least 100 Hz. The 1/f noise profile was worse for the USN (than for the pneumatic nebulizers) regardless of whether or not the NAS were normalized to the d.c. level.

The spray chamber for the USN was very similar to the conical, straight-pass spray chamber described in the last section. The carrier gas for the USN was added through the same drain port as the make-up gas when the Meinhard nebulizer was used with this type of spray chamber. With the Meinhard nebulizer, addition of make-up gas greatly attenuated 1/f noise (*i.e.*, compare Figs. 6, A and 6, B). The USN itself was apparently more susceptible to 1/f noise than the Meinhard nebulizer, because 1/f noise was still substantial with the USN when the same spray chambers were used for either nebulizer. Discrete frequency noise was not noticeable; however, it could have been buried in the 1/f noise.

Conclusions

The present study illustrates several points of practical interest for analysis by ICP-MS or ICP-AES: (*i*) interference noise in nebulization is at relatively low frequencies (*i.e.*, a few Hz) and is caused by pump fluctuations, not by either the nebulizer or spray chamber; (*ii*) the configuration of and gas flow patterns through the spray chamber can affect levels of 1/f noise and white noise. In particular, the common Scott-type chamber suppresses both 1/f noise and white noise, relative to that in the primary aerosol; (*iii*) the ultrasonic nebulizer suffers from additional 1/f noise beyond that expected from the

conical spray chamber usually employed; and (*iv*) the RSD of the scattering signal from the secondary aerosol can be as good as 0.1 %. This value is comparable to the best precision commonly achievable for analytical signals from the ICP in cases where special care is taken to optimize precision. Examples include integrated intensity measurements with a thermostatted spectrometer and Myers-Tracy correction (51) in ICP-AES, or isotope ratio measurements by fast peak hopping in ICP-MS. While the sample introduction system can limit precision of spectrochemical measurements with the ICP, this need not always be the case.

Acknowledgements

The authors gratefully acknowledge Richard Hendrickson of Department of Nuclear Engineering, Iowa State University for the loan of the spectrum analyzer and Stephan J. Weeks for the loan of the laser. The authors thank Royce K. Winge, David E. Eckels, Fred G. Smith, Ke Hu, and Hai-Chou Chang for their helpful discussion and assistance during the course of this work. Ames Laboratory is operated by Iowa State University for the US Department of Energy under Contract No. W-7405-Eng-82. This research was supported by the Office of Basic Energy Sciences, Division of Chemical Sciences.

References

1. Crain, J. S., Houk, R. S., and Eckels, D. E., *Anal. Chem.*, 1989, **61**, 606.

2. Furuta, N., Monnig, C. A., Yang, P., and Hieftje, G. M., *Spectrochim. Acta, Part B*, 1989, **44**, 649.

3. Furuta, N., *J. Anal. At. Spectrom.*, 1991, **6**, 199.

4. Walden, G. L., Bower, J. N., Nikdel, S., Bolton, D. L., and Winefordner, J. D., *Spectrochim. Acta, Part B*, 1980, **35**, 535.

5. Belchamber, R. M., and Horlick, G., *Spectrochim. Acta, Part B*, 1982, **37**, 17.

6. Benetti, P., Bonelli, A., Cambiaghi, M., and Frigieri, P., *Spectrochim. Acta, Part B*, 1982, **37**, 1047.

7. Davies, J., and Snook, R. D., *J. Anal. At. Spectrom.*, 1986, **1**, 195.

8. Davies, J., and Snook, R. D., *J. Anal. At. Spectrom.*, 1987, **2**, 27.

9. Antanavichyus, R. L., Serapinas, P. D., and Shimkus, P. P., *Opt. Spektrosk.*, 1987, **63**, 224.

10. Winge, R. K., Eckels, D. E., DeKalb, E. L., and Fassel, V. A., *J. Anal. At. Spectrom.*, 1988, **3**, 849.

11. Sing, R. L. A., and Hubert, J., *J. Anal. At. Spectrom.*, 1988, **3**, 835.

12. Montaser, A., Ishii, I., Tan, H., Clifford, R. H., and Golightly, D. W., *Spectrochim. Acta, Part B*, 1989, **44**, 1163.

13. Montaser, A., Clifford, R. H., Sinex, S. A., and Capar, S. G., *J. Anal. At. Spectrom.*, 1989, **4**, 499.

14. Goudzwaard, M. P., and De Loos-Vollebregt, M. T. C., *Spectrochim. Acta, Part B*, 1990, **45**, 887.

15. Furuta, N., *Anal. Sci.*, 1990, **6**, 683.

16. Ingle, J. D., Jr., and Crouch, S. R., *Spectrochemical Analysis*, Prentice Hall, Englewood Cliffs, 1988.

17. Olesik, J. W., Smith, L. J., and Williamsen, E. J., *Anal. Chem.* 1989, **61**, 2002.

18. Olesik, J. W., and Fister, J. C., III, *Spectrochim. Acta, Part B,* 1991, **46**, 851.

19. Fister, J. C., III, and Olesik, J. W., *Spectrochim. Acta, Part B,* 1991, **46**, 869.

20. Hobbs, S. E., and Olesik, J. W., *Anal. Chem.*, 1992, **64**, 274.

21. Cicerone, M. T., and Farnsworth, P. B., *Spectrochim. Acta, Part B,* 1989, **44**, 897.

22. Winge, R. K., Crain, J. S., and Houk, R. S., *J. Anal. At. Spectrom.*, 1991, **6**, 601.

23. Browner, R. F., and Boorn, A. W., *Anal. Chem.*, 1984, **56**, 786A and 875A.

24. McGeorge, S. W., and Salin, E. D., *Appl. Spectrosc.*, 1985, **39**, 989.

25. Hobbs, P., Spillane, D. E. M., Snook, R. D., and Thorne, A. P., *J. Anal. At. Spectrom.*, 1988, **3**, 543.

26. Sneddon, J., In *Sample Introduction in Atomic Spectroscopy*, ed. Sneddon, J., Elsevier, Amsterdam, 1990, ch. 1.

27. Montaser, A., Clifford, R. H., and Sohal, P., *Dual-Beam, Light-Scattering Interferometry for Simultaneous Measurements of Droplet-Size and Velocity*

Distributions of Aerosols Produced by New Ultrasonic Nebulizers, 1991 European Winter Conference on Plasma Spectroscopy, Dortmund, Germany, January 1991.

28. Hewlett-Packard, *Operating Manual for Model 3582A Spectrum Analyzer*, Hewlett-Packard, Loveland, 1978.

29. Wiederin, D. R., Smith, F. G., and Houk, R. S., *Anal. Chem.*, 1991, **63**, 219.

30. Wiederin, D. R., Smyczek, R. E., and Houk, R. S., *Anal. Chem.*, 1991, **63**, 1626.

31. Smith, F. G., Wiederin, D. R., and Houk, R. S., *Anal. Chim. Acta*, 1991, **248**, 229.

32. Wiederin, D. R., and Houk, R. S., *Appl. Spectrosc.*, 1991, **45**, 1408.

33. Shum, S. C. K., Neddersen, R., and Houk, R. S., *Analyst*, 1992, **117**, 577.

34. Scott, R. H., Fassel, V. A., Kniseley, R. N., and Nixon, D. E., *Anal. Chem.*, 1974, **46**, 75.

35. Fassel, V. A., and Bear, B. R., *Spectrochim. Acta, Part B*, 1986, **41**, 1089.

36. Hinds, W., and Reist, P. C., *Aerosol Sci.*, 1972, **3**, 501 and 515.

37. Sharp, B. L., *J. Anal. At. Spectrom.*, 1988, **3**, 939.

38. Clifford, R. H., Ishii, I., Montaser, A., and Meyer, G. A., *Anal. Chem.*, 1990, **62**, 390.

39. Belchamber, R. M., and Horlick, G., *Spectrochim. Acta, Part B*, 1981, **36**, 581.

40. Belchamber, R. M., and Horlick, G., *Spectrochim. Acta, Part B*, 1982, **37**, 1075.

41. Boumans, P. W. J. M., and Lux-Steiner, M. Ch., *Spectrochim. Acta, Part B*, 1982, **37**, 97.

42. Schutyser, P., and Janssens, E., *Spectrochim. Acta, Part B*, 1984, **39**, 737.

43. Schutyser, P., and Janssens, E., *Spectrochim. Acta, Part B,* 1979, **34**, 443.

44. Orion Research Inc., *Sage Model 341B Syringe Pump Instruction Manual*, Orion Research Inc., Boston, 1987.

45. Scientific Systems, Inc., *User's Manual for SSI Model 222D Digital HPLC Pump*, Scientific Systems, State College, 1990.

46. Poole, C. F., and Schuette, S. A., *Contemporary Practice of Chromatography*, Elsevier, Amsterdam, 1984.

47. Varian Associates, Inc., *2010 Pump/2210 System Operators Manual*, Varian Instrument, Walnut Creek, 1984.

48. Sprott, J. C., *Introduction to Modern Electronics*, John Wiley & Sons, New York, 1981.

49. Jarvis, K. E., Gray, A. L., and Houk, R. S., *Handbook of Inductively Coupled Plasma Mass Spectrometry*, Blackie, Glasgow, 1992.

50. Fry, R. C., Personal communication, 1992.

51. Myers, S. A., and Tracy, D. H., *Spectrochim. Acta, Part B*, 1983, **38**, 1227.

Table 1 Instrumental components

Component	Manufacturer/description	Operating conditions/specifications
Laser	Melles Griot GreNe green He-Ne cylindrical laser head and power supply (Carlsbad, CA)	Wavelength: 543.5 nm Power: 5 mW Continuous wave
Focusing lens	Rolyn spherical plano-convex glass lens (Covina, CA)	Scattering angle θ: 15°
Iris diaphragm	Edmund precision iris diaphragm (Barrington, NJ)	Aperture: 2.5 mm
Interference filter	Melles Griot He-Ne laser line interference filter (Carlsbad, CA)	Wavelength: 543.5 nm Full width at half maximum: 10 ± 2 nm
PMT	Hamamatsu R 955 side-on type (Japan)	Bias voltage: - 300 V
PMT power supply	Tennelec/Nucleus TC 952 high voltage power supply (Oak Ridge, TN)	—
Spectrum analyzer	Hewlett-Packard Model 3582A (Loveland, CO)	Frequency range: d.c. to ≈ 25 kHz[a] Sensitivity: selects the maximum input level that can be applied to the instrument without overloading Coupling: d.c. Passband shape: Hanning Averaging mode: RMS Number of averages: 4 for 1 Hz, 16 for 10 Hz, 64 for more than 100 Hz

[a] Should be free from alias contamination (28).

Table 1 (continued)

Component	Manufacturer/description	Operating conditions/specifications
X-Y recorder	Houston Omnigraphic Series 2000 (Austin, TX)	—
Picoammeter	Keithley model 485 autoranging picoammeter (Cleveland, OH)	—
Meinhard nebulizer	Meinhard Type TR-30-C3 borosilicate glass concentric nebulizer (Santa Ana, CA)	—
Direct injection nebulizer	Construction as described (29-33)	I.d. of sample delivery capillary: 30 μm
Spray chamber	Scott-type, double-pass spray chamber (34) (Precision Glassblowing, Englewood, CO)	—
	Conical, straight-pass spray chamber (Fig. 7 of Ref. 35, but without any mixing baffle)	—
Ultrasonic nebulizer	Continuous-flow, similar to the designs of Fassel and Bear (35), Model CPMT transducer (Channel Products, Chagrin Falls,OH), Plasma-Therm Model UNPS-1 r.f. power supply (Kresson, NJ)	Resonant frequency of transducer: 1.36 MHz Incident r.f. power: 40 W Reflected r.f. power: 0 - 1 W Liquid flow rate: 2.5 mL min^{-1} Argon carrier gas flow rate: 1.5 L min^{-1}

Table 1 (continued)

Component	Manufacturer/description	Operating conditions/specifications
Peristaltic pump	Gilson Minipuls 2 HP-1 single channel peristaltic pump (Middleton, WI)	—
Syringe pump	Sage Model 341B single channel syringe pump (Orion Research, Boston, MA) with B-D Plastipak syringe (Becton Dickinson, Rutherford, NJ)	—
Single head LC pump	SSI Model 222D digital HPLC pump (Scientific Systems, Inc., State College, PA) with pulse damper	—
Dual head LC pump	Varian 2010 LC pump (Varian Instrument Group, Walnut Greek, CA) with SSI Model LP-21 LO-PULSE pulse damper (Scientific Systems, Inc., State College, PA)	—

Table 2 Pulsation induced by peristaltic pump[a]

Liquid flow rate (mL min^{-1})	Frequency of pulsation (Hz)	Frequency of fundamental noise (Hz)
0.84	0.79	0.80
1.0	0.95	0.96
1.5	1.36	1.36

[a] All frequencies in this table were measured three times; each measurement yielded the same value.

Table 3 Pulsation induced by various pumps[a]

Pump	Liquid flow rate (mL min^{-1})	Frequency of fundamental noise (Hz)
Syringe	0.78	5.2
	1.1	7.2
	1.6	10.8
Single head LC	0.800	0.32
Single head LC + pulse damper	0.800	0.32[b]

[a] All frequencies in this table were measured three times, each measurement yielded the same value.

[b] The amplitude of the pulsation was less severe than when the single head LC pump was used alone (without the pulse damper).

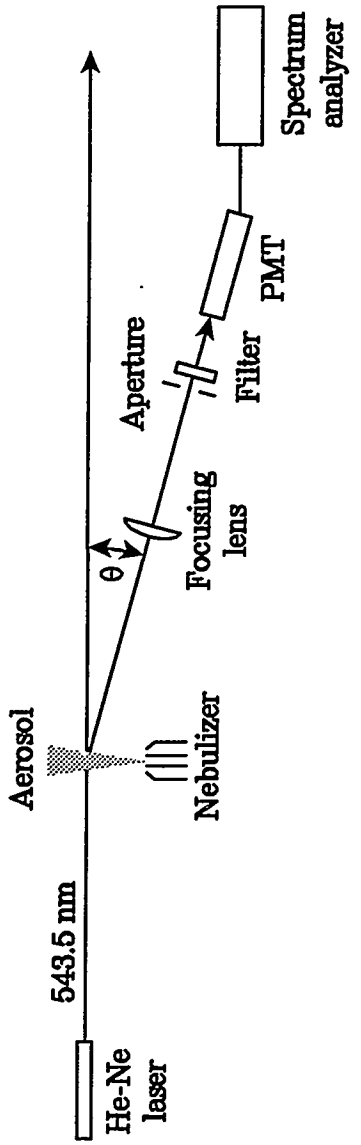

Fig. 1 Block diagram of apparatus used for noise amplitude spectrum measurements

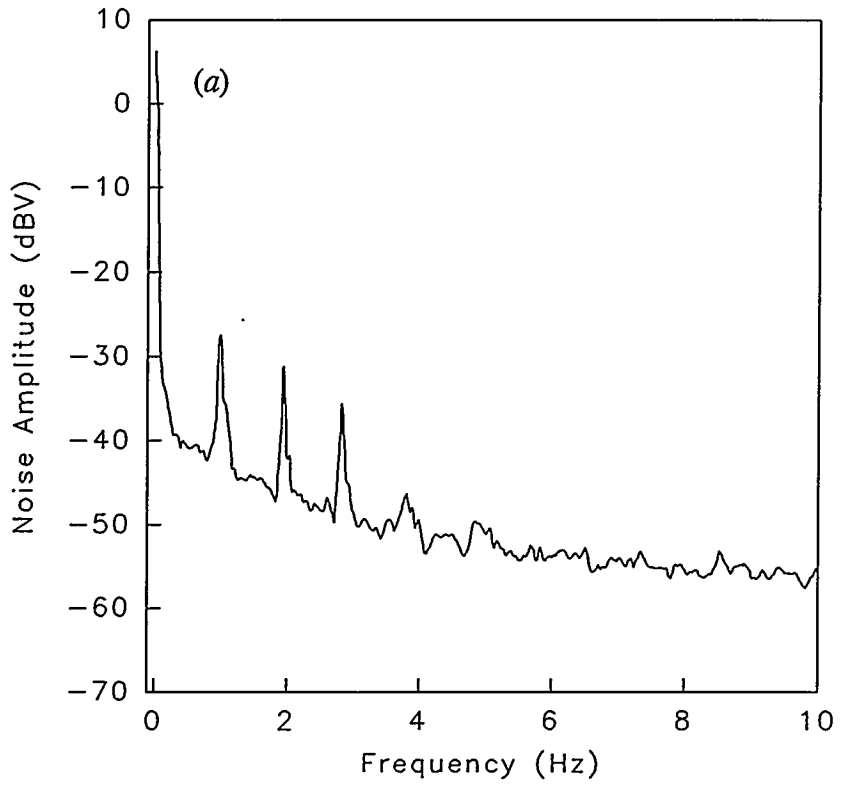

Fig. 2 (*a*) Noise amplitude spectrum of scattering from the primary aerosol generated by a Meinhard nebulizer with a peristaltic pump; and (*b*) noise amplitude spectrum of the primary aerosol generated by a Meinhard nebulizer with self-priming aspiration (natural uptake). No spray chamber was used for either (*a*) or (*b*). The liquid flow rate was 1.0 mL min^{-1}. The argon nebulizer gas flow rate was 1.0 L min^{-1}

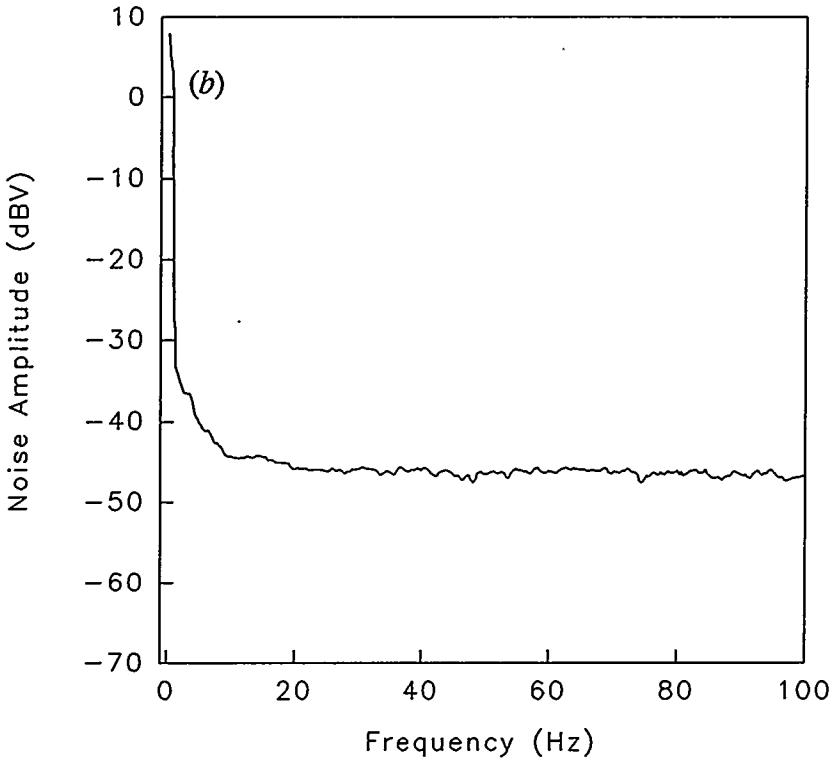

Fig. 2 (continued)

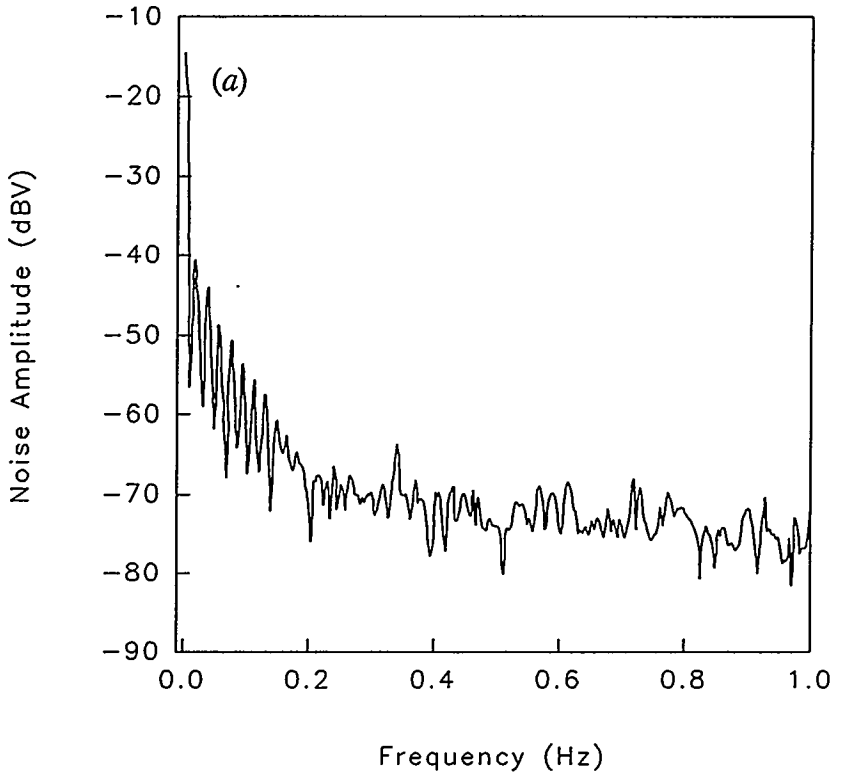

Fig. 3 Noise amplitude spectrum of DIN aerosol with a single head LC pump: (*a*) without the pulse damper; and (*b*) with the pulse damper. The liquid flow rate was 50 μL min^{-1}

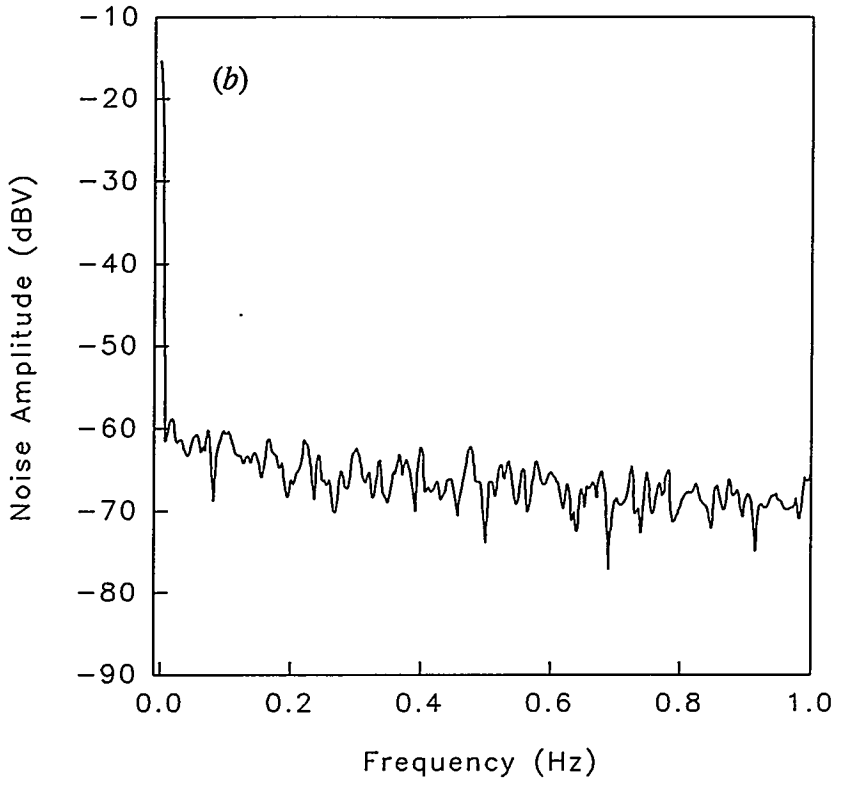

Fig. 3 (continued)

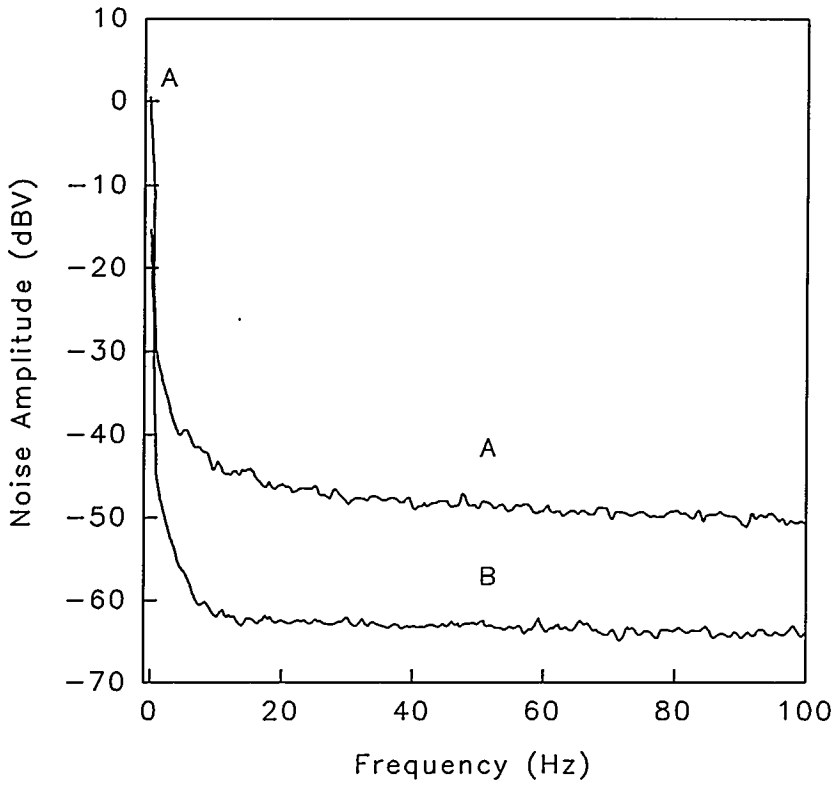

Fig. 4 Comparison between the noise amplitude spectra of the aerosol from A, Meinhard nebulizer (the liquid flow rate was 1.0 mL min^{-1}) and B, a DIN (the liquid flow rate was 50 μL min^{-1}). A dual head LC pump was used in both instances

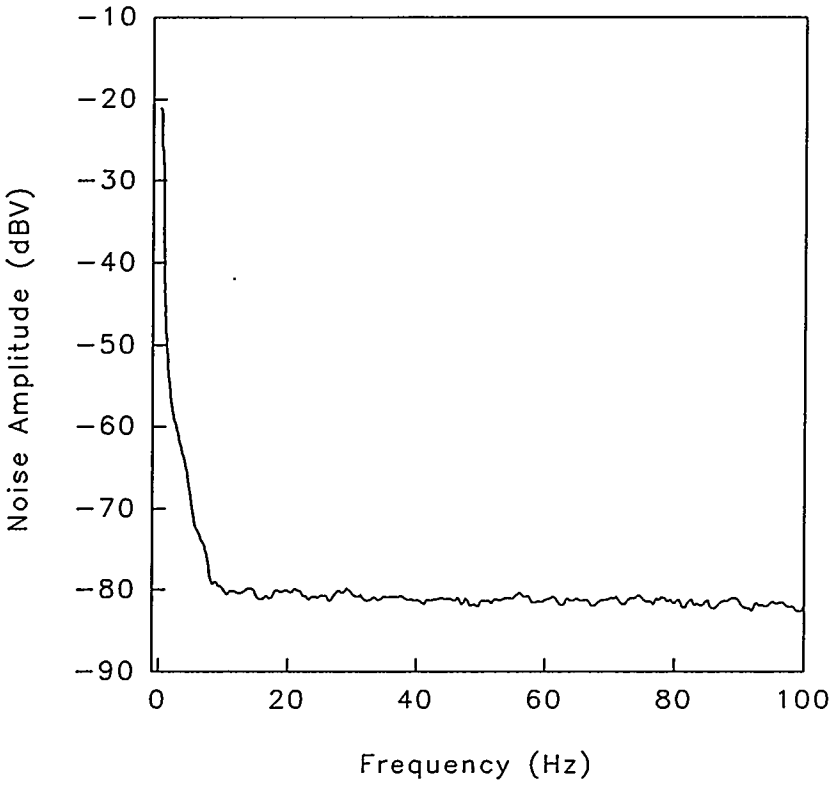

Fig. 5 Noise amplitude spectrum from a Meinhard nebulizer after passage through a Scott-type, double-pass spray chamber. A dual head LC pump was used. The liquid flow rate was 1.0 mL min^{-1}. The argon nebulizer gas flow rate was 1.0 L min^{-1}

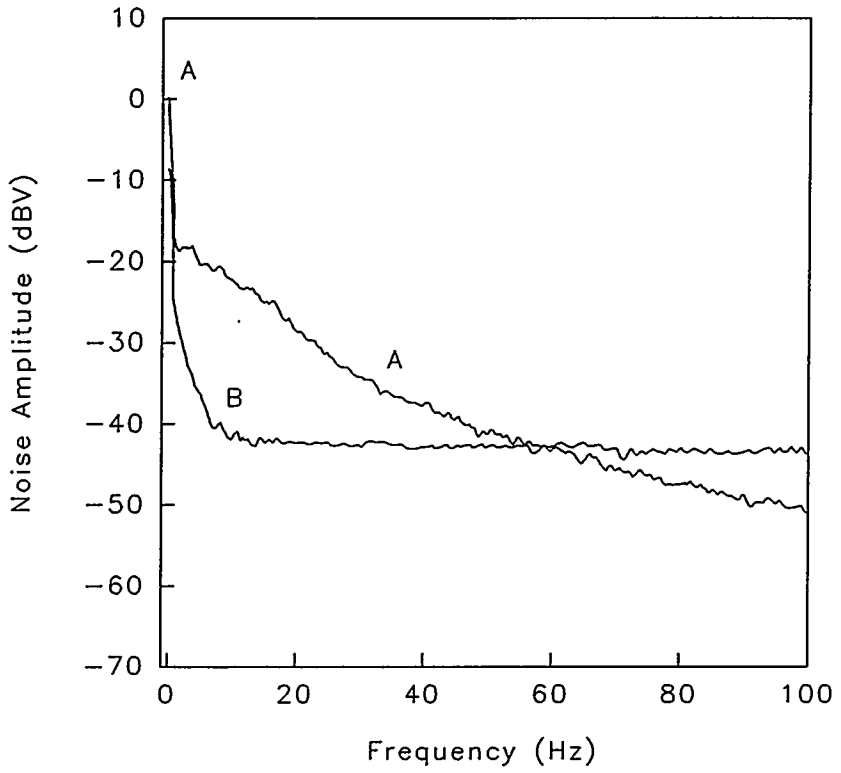

Fig. 6 Noise amplitude spectra from aerosols from a Meinhard nebulizer after passage through a conical, straight-pass spray chamber. A dual head LC pump was used. The liquid flow rate was 1.0 mL min^{-1}. The argon nebulizer gas flow rate was 1.0 L min^{-1}. The argon make-up gas flow rate was: (A) 0; and (B) 0.5 L min^{-1}

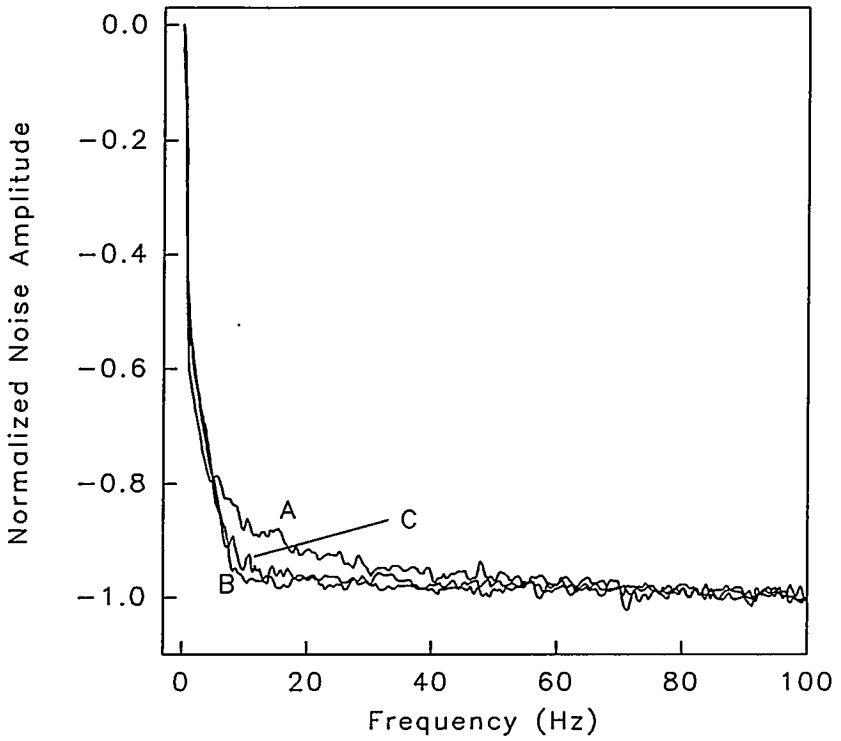

Fig. 7 Normalized noise amplitude spectra of the aerosols from a Meinhard nebulizer alone (A), the same Meinhard nebulizer with a Scott-type, double-pass spray chamber (B), and the same Meinhard nebulizer with a conical, straight-pass spray chamber with make-up gas (C). Each spectrum is normalized to the same white noise level at ≈ 100 Hz. A dual head LC pump was used. The liquid flow rate was 1.0 mL min^{-1}

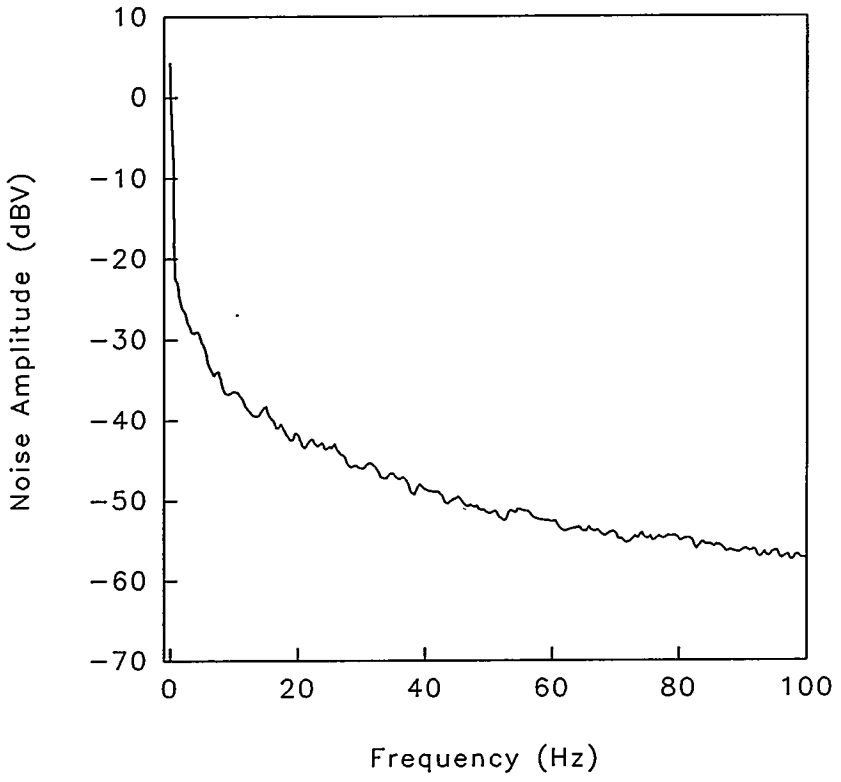

Fig. 8 Noise amplitude spectrum of the aerosol generated by USN (after passage through a straight-pass spray chamber). A dual head LC pump was used. The liquid flow rate was 2.5 mL min^{-1}. The argon carrier gas flow rate was 1.5 L min^{-1}

CHAPTER 3. APPLICATION OF GENERALIZED STANDARD ADDITIONS METHOD TO INDUCTIVELY COUPLED PLASMA ATOMIC EMISSION SPECTROSCOPY WITH AN ECHELLE SPECTROMETER AND SEGMENTED-ARRAY CHARGE-COUPLED DETECTORS

A paper accepted for publication by Spectrochimica Acta, Part B, Atomic Spectroscopy

Shen Luan, Ho-ming Pang, and R. S. Houk[1]

Abstract

Simultaneous correction for both spectral interferences and matrix effects in inductively coupled plasma atomic emission spectrometry (ICP-AES) can be accomplished by using the generalized standard additions method (GSAM). Results obtained with the application of the GSAM to the Perkin-Elmer Optima 3000 ICP atomic emission spectrometer are presented. The echelle-based polychromator with segmented-array charge-coupled device detectors enables the direct, visual examination of the overlapping lines Cd (I) 228.802 nm and As (I) 228.812 nm. The slit translation capability allows a large number of data points to be sampled, therefore, the advantage of noise averaging is gained. Pure spectra of each of the spectrally active components in the sample can be extracted through the GSAM calculation.

---

[1] Author to whom correspondence should be addressed.

Introduction

Correcting for spectral interferences in inductively coupled plasma atomic emission spectrometry (ICP-AES) using chemometric approaches has recently emerged as an attractive alternative to tedious matrix separation or resorting to less sensitive lines. Various multivariate methods for handling overlapping spectra in ICP-AES have been proposed, including Kalman filtering [1-9], ordinary least squares (OLS) [10-12], multicomponent spectral fitting (MSF) [13, 14], stepwise multiple linear regression (MLR) [15], numerical derivatives [16-18], curve resolution [19, 20], orthogonal polynomials [21], factor analysis [22-24], and neural networks [25]. These multivariate methods take advantage of the multi-wavelength and the linear response characteristics of ICP atomic emission spectra [26-29] by using linear mathematics. The advantages of using these multivariate methods include: (*i*) correction for spectral interferences, (*ii*) built-in background correction superior to off-line methods, (*iii*) detection and correction of wavelength position errors which are often omnipresent in sequential spectrometers, (*iv*) noise averaging resulting from the use of all the data points available in a spectrum, and (*v*) the availability of a residuals vector that can be used to evaluate the quality of the analytical determination and identify unexpected interferences [13, 14]. One requirement of these multivariate methods, however, is that all analytes and all interferences must be known in advance, so that a model containing pure spectra of each of the expected components in the unknown sample can be constructed [13, 14].

Another disadvantage with the multivariate methods mentioned above is that they generally do not correct for non-spectroscopic matrix effects [3, 30], unless special efforts are made to measure intensities with the matrix present [4]. However, it is well known that these matrix effects can be eliminated by using the standard additions method. The generalized standard additions method (GSAM) developed by Saxberg and Kowalski [31] is a multivariate extension of the conventional standard additions method for simultaneous multicomponent determinations. The GSAM looks promising as a method by which both the spectral interferences and the matrix effects can be overcome simultaneously. However, considerable effort is needed to make standard additions for all the analytes in multielement determinations. The use of discontinuous flow analysis (DFA) [30, 32, 33] considerably reduces the time and labor involved in constructing such multielement calibration standards.

The GSAM has been applied to ICP-AES for simultaneous correction for spectral interferences and matrix effects [34-36]. In these studies, the direct-reading spectrometer with an array of slits and photomultipliers was used. A certain number of spectral lines at fixed, pre-set wavelengths were measured simultaneously. Due to the limitation of the direct-reading spectrometer used in these studies, no spectrum was recorded for visual inspection of the spectral interferences studied. In addition, the number of data points collected in the wavelength coordinate within a given spectral window plays an important role in the calculations required for the GSAM. A large number of data points improves signal-to-noise ratios because measurement of the entire line profile provides an overdetermined system [37]. With the fairly limited number of channels available in the

direct-reading spectrometer used in these earlier studies [34-36], the number of data points collected was restricted.

In this present paper, a case study of how the GSAM can be applied to an echelle-based polychromator with two segmented-array charge-coupled device detectors (SCD) [38, 39] is provided. The echelle grating optical system with two-dimensional, multichannel solid-state detectors offers a convenient way to implement spectral scans for the GSAM. In particular, scans over 56 wavelength intervals for each subarray of the SCD can be generated by moving the entrance slit only 4 times. Spectra can be scanned in much the same way with a direct-reading spectrometer by the common practice of translating the entrance slit, but the entrance slit must be moved once for each wavelength interval desired around the lines of interest. This procedure was not used in the earlier GSAM studies [34-36]. Of course, either the direct reader or the echelle spectrometer can implement a multielement GSAM scheme much more rapidly than a scanning monochromator.

Theoretical

The background and theory of the GSAM and its different versions have been discussed in full detail by Kowalski and co-workers [31, 34, 35, 37, 40-43]. Therefore, only a short overview is given here.

For r analytes, the responses from p pixels are recorded before and after n standard additions are made. The model in matrix notation is

$$R = CK \quad \ldots\ldots\ldots\ldots\ldots\ldots\ldots\ldots \quad (1)$$

where R is a $(n + 1) \times p$ matrix made up of $n + 1$ rows corresponding to the reading for the original sample solution plus readings made after each of the n standard additions. Each of the p columns of R stands for a different pixel. The $(n + 1) \times r$ matrix C is a matrix of concentrations consisting of $n + 1$ rows for the original sample concentration plus n additions for each of the r analytes. The $r \times p$ matrix K is a matrix of sensitivities, in counts per second per unit concentration, for each of the r analytes at the p pixels. Since concentrations are not always additive, using *volume-corrected changes* for the responses [40], equation (1) becomes

$$\Delta Q = \Delta NK \quad \ldots\ldots\ldots\ldots\ldots\ldots\ldots\ldots \quad (2)$$

where ΔQ is now the $n \times p$ volume-corrected response change matrix and ΔN is the $n \times r$ absolute quantity matrix (*e.g.*, μg) of standards added to the original sample. By use of the method of multiple linear least squares to solve for K in the presence of an overdetermined system ($n > r$), the *generalized inverse* of ΔN [43, 44] is needed resulting in

$$K = (\Delta N^T \Delta N)^{-1} \Delta N^T \Delta Q \quad \ldots\ldots\ldots\ldots\ldots\ldots \quad (3)$$

where the generalized inverse of the matrix ΔN is defined as $(\Delta N^T \Delta N)^{-1} \Delta N^T$, the superscript T signifies the transpose matrix, and the superscript "-1" indicates the inverse

matrix operation. After calculation of the K matrix, the vector of initial analyte quantities n_0 is recovered [42, 43] for the case of $p > r$ by solving

$$n_0 = q_0 K^T (K K^T)^{-1} \quad \ldots\ldots\ldots\ldots\ldots\ldots \quad (4)$$

where q_0 is the volume-corrected initial response vector.

The matrix ΔN used in the present study is based upon partition GSAM (PGSAM) [40] design as shown in Table 1. The corresponding ΔQ matrix is based upon a total difference calculation (TDC) method [40]. The ΔQ entries are total changes in response from q_0.

Experimental

Apparatus

The instrument used in the present study was a Perkin-Elmer Optima 3000 ICP atomic emission spectrometer. Table 2 summarizes the instrumental components.

Translating the slit shifts the image spectrum across the subarray to increase the number of data points sampled within a given spectral window [38]. Four independent exposures with the slit translated in steps of ¼ slit width are required for this operating mode. The resulting spectrum has uniform spacing in the wavelength coordinate and four times the number of data points as compared to a spectrum collected with a single exposure and a stationary slit (scanning off mode) [14].

Because of the high wavelength stability of this instrument [14, 38], no correction for wavelength drift was necessary. The automatic mercury wavelength recalibration lamp

was turned off during the course of the GSAM measurement. Results in this study supported the conclusion that the wavelength drift was negligible.

The case studied is the overlap of As (I) 228.812 nm on Cd (I) 228.802 nm, which has been described in the literature [5, 25, 34, 38]. The separation between the peak maxima is $\sim$10 pm. This is the strongest Cd line emitted by the ICP; the As line is one of the strongest among only a few mediocre lines for this element [45]. The spectral resolution is $\sim$9 pm (FWHM) in this wavelength region with the entrance slit width used in this present study (*i.e.*, 62 μm) [38].

The Optima 3000 software version 1.2 was used to acquire the spectral data. However, the results were processed off-line. Lotus 1-2-3 for DOS (Release 2.4) (Lotus Development, Cambridge, MA) spreadsheet software was used to carry out all the matrix operations.

Reagents

For As and Cd, ICP single element stock solutions (PLASMA-CHEM, Farmingdale, NJ) with concentrations of 1000 μg mℓ^{-1} in 2% (v/v) HNO_3 were used. For Na, an ICP single element stock solution (SPEX, Edison, NJ) with concentration of 10000 μg mℓ^{-1} in 5% (v/v) HNO_3 was used. All solutions were prepared using 18 MΩ·cm deionized water and double distilled nitric acid at 2% (v/v) (GFS Chemicals, Powell, OH).

Procedure

As-Cd sample I. Seven 10.00-mℓ test sample aliquots with concentrations of 52.00 μg mℓ^{-1} As and 0.950 μg mℓ^{-1} Cd were prepared. The spikes consisted of one addition of a single analyte per test sample aliquot with a total of three aliquots for each analyte. The three aliquots per analyte received 500, 1000, and 1500 $\mu\ell$ of the respective analyte standard. The concentrations of the prepared standards were 1000 μg mℓ^{-1} As and 20.00 μg mℓ^{-1} Cd.

Other samples. The same additions procedure as in As-Cd sample I was used except the concentrations of the components of the original test samples were different, as listed in Table 3.

Results and Discussion

Preliminary evaluation of the GSAM for the Optima 3000

Preliminary experiments were carried out using As-Cd sample I. Figure 1 shows the spectra for the original sample solution and after each of the 6 standard additions. The continuum background has been subtracted from these and subsequent spectra. The spectra are composed of 56 data points and represent all the spectral information available from subarray 63. For the spectrum of the original sample solution [Fig. 1(a)], the large As (I) 228.812 nm interference on Cd (I) 228.802 nm is obvious. The spectra recorded after each of the standard additions [Fig. 1(b)-(g)] allow the direct, visual examination of the two overlapping spectral lines studied.

The GSAM was then applied to these data. The first step in the GSAM calculation is the evaluation of the K matrix [equation (3)]. The K matrix is a matrix of sensitivities, in counts per second per unit concentration. The 2 rows represent 2 analytes in the matrix, As and Cd. The 56 columns show the contribution of each of the 2 analytes to the 56 data points collected in the wavelength coordinate. Each row of K is plotted here in Fig. 2. Each plot here corresponds to the pure spectrum of each analyte, but they are taken from a 2-component solution, not from individual components. The observed wavelengths for cadmium (228.802 nm) and arsenic (228.812 nm) are in good agreement ($\pm$ 0.001 nm) with wavelengths measured from single element solutions and with various wavelength tables [45].

The final results of the GSAM calculation for the As-Cd sample I are shown in Table 4. The observed initial analyte quantities (n_0) agree closely with the true n_0 vector.

In addition, a spectrum that is an estimate of the composition of the original sample solution can be reconstructed from the GSAM calculation by using the following equation:

$$r_0 = c_0 K \quad \ldots\ldots\ldots\ldots\ldots\ldots\ldots\ldots \quad (5)$$

where K is the matrix of sensitivities from equation (3), c_0 is the vector of the true initial analyte concentrations (in this case, 0.950 μg mℓ^{-1} Cd and 52.00 μg mℓ^{-1} As, respectively), and r_0 is the reconstructed initial response vector. As a check on the validity of the GSAM calculation, Figure 3 compares the experimental spectrum (solid line) for the original sample solution with the reconstructed spectrum based on the GSAM calculation (filled circles). The experimental spectrum conforms

closely to the reconstructed spectrum, as shown clearly in Fig. 3. The plot shown at the bottom of Fig. 3 is a vertically expanded plot of the residuals vector. The small hump around 228.812 nm accounts for the 0.75% relative error in n_0 for As, as shown in Table 4.

Accuracy and precision of the GSAM for As-Cd samples

The GSAM was tested extensively by using As-Cd samples II, III, and IV (Table 3). Five measurements were made for each sample (using the same set of 7 test sample solutions). No mercury wavelength recalibration was done within each GSAM measurement (*i.e.*, from the original sample solution to the last standard addition solution). The mercury wavelength recalibrations were carried out only between each of the GSAM measurements. The measured wavelengths were highly stable, and this recalibration was probably not necessary.

Table 5 lists the GSAM calculated values for n_0 (initial analyte quantities) with corresponding relative standard deviations (RSD) and the relative errors. A precision of 1.3 - 4.2% with an accuracy of 1.0 - 3.4% absolute error was achieved (Table 5).

The spectral characteristics of the case studied here are favorable for this mathematical treatment. The intensity ratios of cadmium to arsenic are 0.96, 0.44, and 0.32 for As-Cd samples II, III, and IV, respectively. However, as shown in Table 5, the relative errors do not degrade at lower intensity ratios. It is clear that the initial analyte quantities are properly estimated by the GSAM over the range of intensity ratios studied.

Also in the case studied here, the peak separation is rather large ($\sim$10 pm), which is comparable to the spectral bandwidth of the spectrometer ($\sim$9 pm). The GSAM will not correct for a direct spectral overlap. Some peak separation is required for accurate estimation of the initial analyte quantities. In the present study, the necessary peak separation required for accurate results was not evaluated. However, in other studies using Kalman filtering in ICP-AES [2], the necessary peak separation was found to be at least 2 or 3 intervals in the wavelength coordinate between the peak maxima. The 10-pm peak separation between these Cd and As lines corresponds to 5 wavelength intervals. The term "wavelength interval" refers to the mininum measurable separation along the wavelength coordinate [2]. For this apparatus, the wavelength interval is ¼ of the pixel width (in wavelength units), since the entrance slit is moved to four different locations.

Correction for matrix effects using GSAM

The ultimate advantage of the GSAM over other multivariate methods is that both spectral interferences and matrix effects can be overcome simultaneously. Table 6 shows the accuracy and the precision of the GSAM for the As-Cd-Na samples. In these samples, sodium serves as a matrix. The Na concentrations were 1000, 2000, and 3000 μg mℓ^{-1} for As-Cd-Na samples I, II, and III, respectively. No detectable amount of Cd and As was found in a matrix blank (3000 μg mℓ^{-1} Na). As shown in Table 6, the absolute error was less than 1.4% in all cases, with a precision within 2.2% RSD.

Figure 4 shows the effect of Na on the intensities of these Cd and As lines. These spectra were extracted through the GSAM calculation [*i.e.*, equation (3)]. The Na matrix

concentrations were 0, 1000, 2000, and 3000 μg mℓ^{-1} for the four solutions studied. As can be seen from Fig. 4, both Cd and As intensities were suppressed, to somewhat different extents, by the Na matrix by up to $\sim$20% of their initial intensities. The results shown here illustrate that accurate corrections for moderate matrix effects can be accomplished by using the GSAM. Internal standardization would probably not yield an interference correction of this quality, unless substantial effort was devoted to selecting an element and line that is suppressed by an amount just intermediate between that seen for the two analyte lines.

The pair of lines presented in this paper has been studied by using the GSAM with a direct-reading ICP spectrometer [34]. However, no effort was made to investigate matrix effects, although it was claimed that the GSAM can simultaneously correct for spectral interferences and matrix effects [34].

Time required for the GSAM

One disadvantage of the GSAM, however, is the time and effort required for the spiking procedure. In this case, each sample requires 6 standard additions. The time involved in constructing such a set of 6 solutions is $\sim$10 minutes. The measurement time from the original sample solution to the last standard addition solution is $\sim$10 minutes. The GSAM calculation time is $\sim$15 minutes with the spreadsheet software used in this present study. However, with the help of a more sophisticated multivariate software package, the GSAM calculation time can be considerably reduced to about 30 seconds [30]. The real potential of the GSAM will be realized when the standard

additions are automated. The flow injection method for on-line standard additions with the direct injection nebulizer (DIN) [46] and discontinuous flow analysis (DFA) system [30, 32, 33] look promising in this regard, although any standard additions method will undoubtedly still be slower than external calibration with analogous hardware and sample handling.

Conclusions

It has been shown in this case study that the GSAM can be applied to an echelle-based polychromator with segmented-array charge-coupled device detectors (SCD), which enables the direct, visual examination of some overlapping spectral lines. The slit translation capability samples a large number of data points (in this case, 56 data points) at fine wavelength intervals within a given spectral window. Therefore, all spectral information available throughout the spectrum can be used to reduce the noise by signal averaging. Pure spectra of each of the components in the sample can be extracted through the GSAM calculation. The validity of the GSAM is confirmed by comparison of the experimental spectrum of the original sample solution with the GSAM reconstructed spectrum. The results are encouraging.

Limitations of the GSAM include: (*i*) the need to know the approximate amount of analyte in the sample, so the proper amount of spike can be used, and (*ii*) the time, effort, and potential for contamination associated with multielement spikes. In particular, if overlap between lines of three or more elements is a problem, then more spike

additions become necessary, beyond the 6 spikes that suffice in the present work. We are currently evaluating these potential problems for multielement analysis, particularly for cases in which one of the overlapping lines is much weaker than the other.

The present form of the GSAM will not correct for a completely unknown spectral interference. A promising approach for overcoming the limitation of the GSAM is the generalized rank annihilation method (GRAM), which can be used to correct for unexpected spectral interferences [47-49]. For GRAM, a second-order bilinear instrument must be available. A new chemometric approach that can predict the presence of an interfering line when the sample composition is not known has been described [50]. Also, heuristic and statistical algorithms for automated spectral background estimation were presented and evaluated recently [51].

Acknowledgements

The authors gratefully acknowledge The Perkin-Elmer Corporation for the loan of the Optima 3000 atomic emission spectrometer. The authors thank Dr. Dennis A. Yates of The Perkin-Elmer Corporation for his help in acquisition of the spectral data in the ASCII format. Ames Laboratory is operated by Iowa State University for the U.S. Department of Energy under Contract No. W-7405-Eng-82. This research was supported by the Office of Basic Energy Sciences, Division of Chemical Sciences.

References

[1] E. H. van Veen and M. T. C. de Loos-Vollebregt, *Spectrochim. Acta* **45B**, 313 (1990).

[2] E. H. van Veen, F. J. Oukes and M. T. C. de Loos-Vollebregt, *Spectrochim. Acta* **45B**, 1109 (1990).

[3] E. H. van Veen and M. T. C. de Loos-Vollebregt, *Anal. Chem.* **63**, 1441 (1991).

[4] E. H. van Veen, M. T. C. de Loos-Vollebregt, A. P. Wassink and H. Kalter, *Anal. Chem.* **64**, 1643 (1992).

[5] E. H. van Veen, S. Bosch and M. T. C. de Loos-Vollebregt, *Spectrochim. Acta* **48B**, 1691 (1993).

[6] J. Yang, Z. Piao, X. Zeng, Z. Zhang and X. Chen, *Spectrochim. Acta* **47B**, 1055 (1992).

[7] J. Yang, Z. Piao and X. Zeng, *Appl. Spectrosc.* **46**, 1816 (1992).

[8] J. Yang, Z. Piao and X. Zeng, *Spectrochim. Acta* **48B**, 359 (1993).

[9] J. Yang, Z. Piao and X. Zeng, *Spectrochim. Acta* **48B**, 543 (1993).

[10] G. Bauer, W. Wegscheider and H. M. Ortner, *Fresenius J. Anal. Chem.* **340**, 135 (1991).

[11] G. Bauer, W. Wegscheider and H. M. Ortner, *Spectrochim. Acta* **46B**, 1185 (1991).

[12] G. Bauer, W. Wegscheider and H. M. Ortner, *Spectrochim. Acta* **47B**, 179 (1992).

[13] J. C. Ivaldi, D. Tracy, T. W. Barnard and W. Slavin, *Spectrochim. Acta* **47B**, 1361 (1992).

[14] J. C. Ivaldi and T. W. Barnard, *Spectrochim. Acta* **48B**, 1265 (1993).

[15] M. Glick, K. R. Brushwyler and G. M. Hieftje, *Appl. Spectrosc.* **45**, 328 (1991).

[16] P. Taylor and P. Schutyser, *Spectrochim. Acta* **41B**, 81 (1986).

[17] G. Bauer, I. Rehana, W. Wegscheider and H. M. Ortner, *Spectrochim. Acta* **43B**, 971 (1988).

[18] J. Yang, Z. Piao and X. Zeng, *Spectrochim. Acta* **46B**, 953 (1991).

[19] A. Lorber, Z. Goldbart and A. Harel, *Anal. Chem.* **57**, 2537 (1985).

[20] A. Lorber, A. Harel, Z. Goldbart and I. B. Brenner, *Anal. Chem.* **59**, 1260 (1987).

[21] S. M. Hassan and N. T. Loux, *Spectrochim. Acta* **45B**, 719 (1990).

[22] D. F. Wirsz and M. W. Blades, *Anal. Chem.* **58**, 51 (1986).

[23] D. F. Wirsz and M. W. Blades, *Talanta* **37**, 39 (1990).

[24] Z. Zhang, Z. Piao and X. Zeng, *Spectrochim. Acta* **48B**, 403 (1993).

[25] C. Schierle and M. Otto, *Fresenius J. Anal. Chem.* **344**, 190 (1992).

[26] K. R. Beebe and B. R. Kowalski, *Anal. Chem.* **59**, 1007A (1987).

[27] E. V. Thomas, *Anal. Chem.* **66**, 795A (1994).

[28] H. Martens and T. Naes, *Trends Anal. Chem.* **3**, 204 (1984).

[29] T. Naes and H. Martens, *Trends Anal. Chem.* **3**, 266 (1984).

[30] M. Selby, *At. Spectrosc.* **15**, 27 (1994).

[31] B. E. H. Saxberg and B. R. Kowalski, *Anal. Chem.* **51**, 1031 (1979).

[32] G. M. Kimber, B. L. Krieger, M. Selby, F. O. Smith, E. E. Turak, J. D. Petty and R. M. Peachey, *Chem. Aust.* **60**, 172 (1993).

[33] B. L. Krieger, G. M. Kimber, M. Selby, F. O. Smith, E. E. Turak, J. D. Petty and R. M. Peachey, *J. Anal. At. Spectrom.* in press.

[34] J. H. Kalivas and B. R. Kowalski, *Anal. Chem.* **53**, 2207 (1981).

[35] J. H. Kalivas and B. R. Kowalski, *Anal. Chem.* **54**, 560 (1982).

[36] A. S. Al-Ammar, H. A. Hamid and B. H. Rashid, *Spectrochim. Acta* **45B**, 359 (1990).

[37] J. H. Kalivas, *Anal. Chem.* **55**, 565 (1983).

[38] T. W. Barnard, M. I. Crockett, J. C. Ivaldi and P. L. Lundberg, *Anal. Chem.* **65**, 1225 (1993).

[39] T. W. Barnard, M. I. Crockett, J. C. Ivaldi, P. L. Lundberg, D. A. Yates, P. A. Levine and D. J. Sauer, *Anal. Chem.* **65**, 1231 (1993).

[40] C. Jochum, P. Jochum and B. R. Kowalski, *Anal. Chem.* **53**, 85 (1981).

[41] J. H. Kalivas and B. R. Kowalski, *Anal. Chem.* **55**, 532 (1983).

[42] I. E. Frank, J. H. Kalivas and B. R. Kowalski, *Anal. Chem.* **55**, 1800 (1983).

[43] E. Sanchez and B. R. Kowalski, *J. Chemometrics* **2**, 247 (1988).

[44] J. Neter and W. Wasserman, *Applied Linear Statistical Models*. Richard D. Irwin, Inc., Homewood, IL (1974), Chap. 6.

[45] R. K. Winge, V. A. Fassel, V. J. Peterson and M. A. Floyd, *Inductively Coupled Plasma-Atomic Emission Spectroscopy: An Atlas of Spectral Information*, Elsevier, New York (1985).

[46] D. R. Wiederin, R. E. Smyczek and R. S. Houk, *Anal. Chem.* **63**, 1626 (1991).

[47] E. Sanchez and B. R. Kowalski, *Anal. Chem.* **58**, 496 (1986).

[48] E. Sanchez and B. R. Kowalski, *J. Chemometrics* **2**, 265 (1988).

[49] K. S. Booksh and B. R. Kowalski, *Anal. Chem.* **66**, 782A (1994).

[50] P. Zhang, D. Littlejohn and P. Neal, *Spectrochim. Acta* **48B**, 1517 (1993).

[51] M. L. Salit, J. B. Collins and D. A. Yates, *At. Spectrosc.* **48**, 915 (1994).

Table 1. Standard additions matrix ΔN used in GSAM experiments

Addition	Cd (μg)	As (μg)
1	10	0
2	20	0
3	30	0
4	0	500
5	0	1000
6	0	1500

Table 2. Instrumental components

Component	Manufacturer/description	Operating conditions/specifications
ICP generator	Perkin-Elmer Optima 3000 40-MHz free-running RF generator with True Power Control	RF power: 1100 W
ICP torch	Perkin-Elmer Optima 3000 demountable torch with 2.0-mm i.d. alumina injector	Plasma argon flow: 15 ℓ min^{-1} Auxiliary argon flow: 1.0 ℓ min^{-1}
Nebulizer	GemTip cross-flow nebulizer	Nebulizer argon flow: 1.000 ℓ min^{-1}
Spray chamber	Ryton Scott-type, double-pass spray chamber with pumped drain	
Peristaltic pump	Gilson Minipuls 3 two channel peristaltic pump	Sample (water) pump rate: 1.0 mℓ min^{-1} I.d. of sample pump tubing: 0.76 mm
Spectrometer	Perkin-Elmer Optima 3000 echelle-based polychromator with two segmented-array, charge-coupled device detectors (SCD)	Viewing height: 15 mm above load coil Slit scanning: 4 interleaved exposures Resolution: Normal Integration time: 10 seconds per exposure Emission line: Cd 228.802 nm Subarray: #63 Data points: 56 Wavelength drift correction: None

Table 3. Concentrations of all components of the original test samples prepared

		Cd ($\mu g\ m\ell^{-1}$)	As ($\mu g\ m\ell^{-1}$)	Na ($\mu g\ m\ell^{-1}$)
As-Cd	sample I	0.950	52.00	0
As-Cd	sample II	1.000	25.00	0
As-Cd	sample III	1.000	55.00	0
As-Cd	sample IV	1.000	75.00	0
As-Cd-Na	sample I	1.000	55.00	1000
As-Cd-Na	sample II	1.000	55.00	2000
As-Cd-Na	sample III	1.000	55.00	3000

Table 4. Final results of the GSAM calculation for the As-Cd sample I

	True n_0 (μg)	Observed n_0 (μg)	Relative error (%) [a]
Cd	9.50	9.48	0.2
As	520.0	523.9	0.75

[a] Relative error = 100 × (| true - observed |)/true.

Table 5. Accuracy and precision of the GSAM for As-Cd samples

	True n_0 (μg)	Observed n_0 (μg) [a]	RSD (%) [b]	Relative error (%) [c]
As-Cd sample II				
Cd	10.00	10.03	1.8	1.3
As	250.0	247.1	4.2	3.4
As-Cd sample III				
Cd	10.00	10.00	1.5	1.2
As	550.0	553.2	1.3	1.0
As-Cd sample IV				
Cd	10.00	10.14	2.5	2.1
As	750.0	744.0	2.5	2.1

[a] Average of five measurements.

[b] Derived from five measurements.

[c] Relative error = 100 × (| true - observed |)/true. Average of five relative errors.

Table 6. Accuracy and precision of the GSAM for As-Cd-Na samples

	True n_0 (μg)	Observed n_0 (μg) [a]	RSD (%) [b]	Relative error (%) [c]
As-Cd-Na sample I				
Cd	10.00	9.99	1.5	1.2
As	550.0	549.4	1.2	1.0
As-Cd-Na sample II				
Cd	10.00	10.04	1.4	1.1
As	550.0	551.2	0.9	0.8
As-Cd-Na sample III				
Cd	10.00	9.95	2.2	1.4
As	550.0	555.4	1.0	1.0

[a] Average of five measurements.

[b] Derived from five measurements.

[c] Relative error = 100 × (| true - observed |)/true. Average of five relative errors.

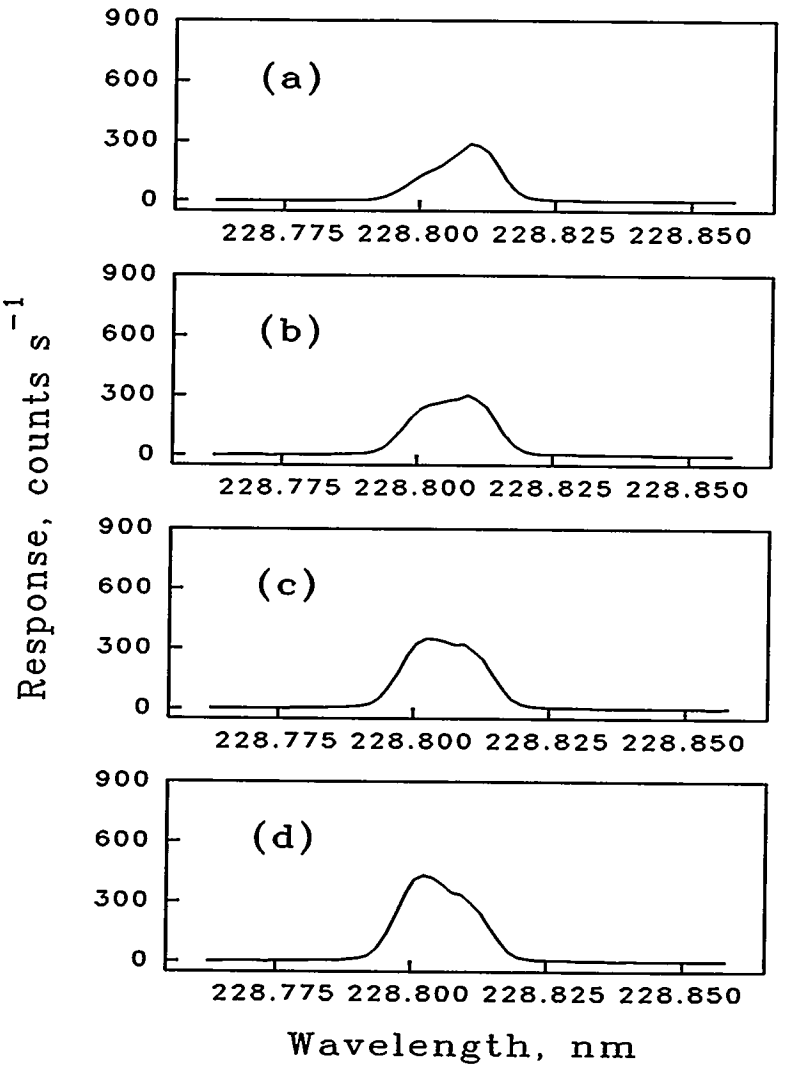

Fig. 1. Spectra of Cd (I) 228.802 nm and As (I) 228.812 nm for (a) original sample solution and after addition of (b) 10 μg Cd; (c) 20 μg Cd; (d) 30 μg Cd; (e) 500 μg As; (f) 1000 μg As; or (g) 1500 μg As.

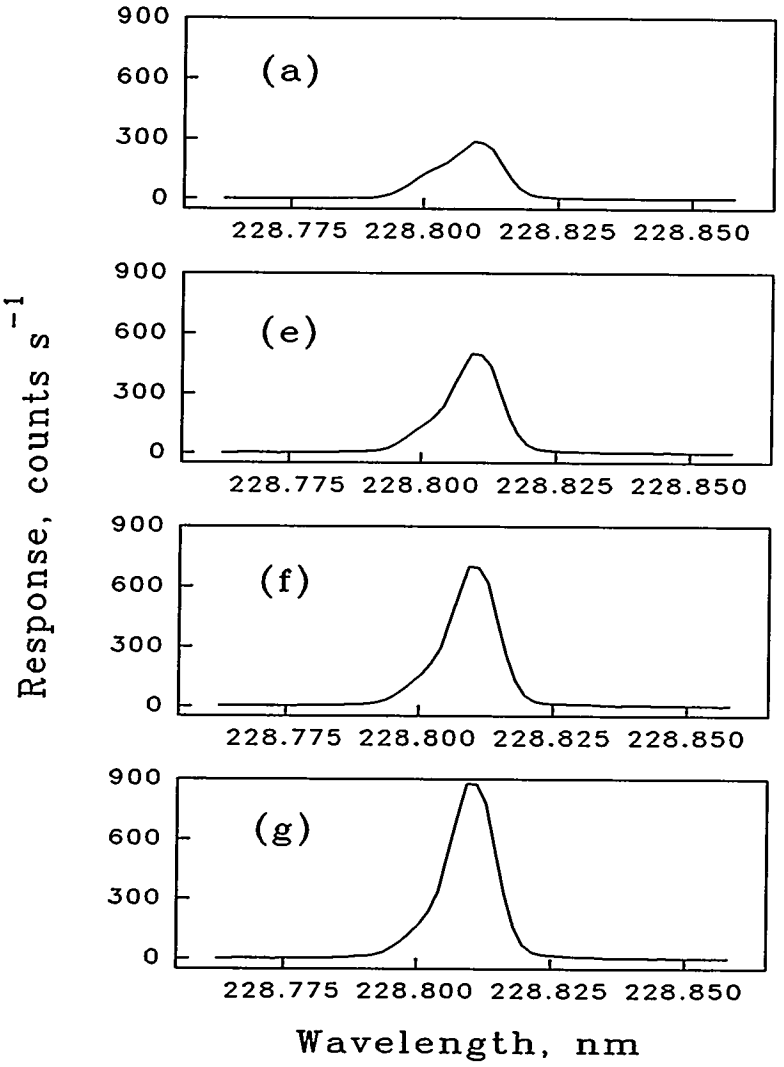

Fig. 1. (continued)

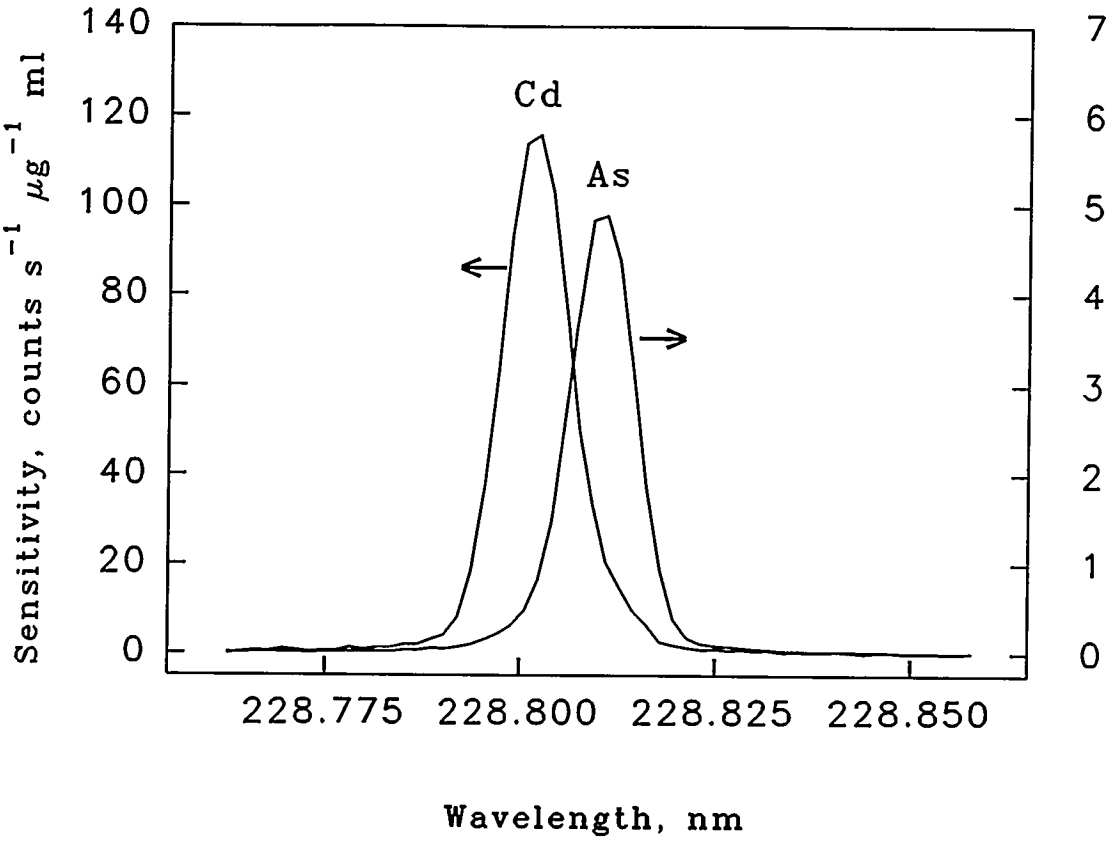

Fig. 2. The pure spectra of individual components extracted from GSAM calculation obtained from As-Cd sample I.

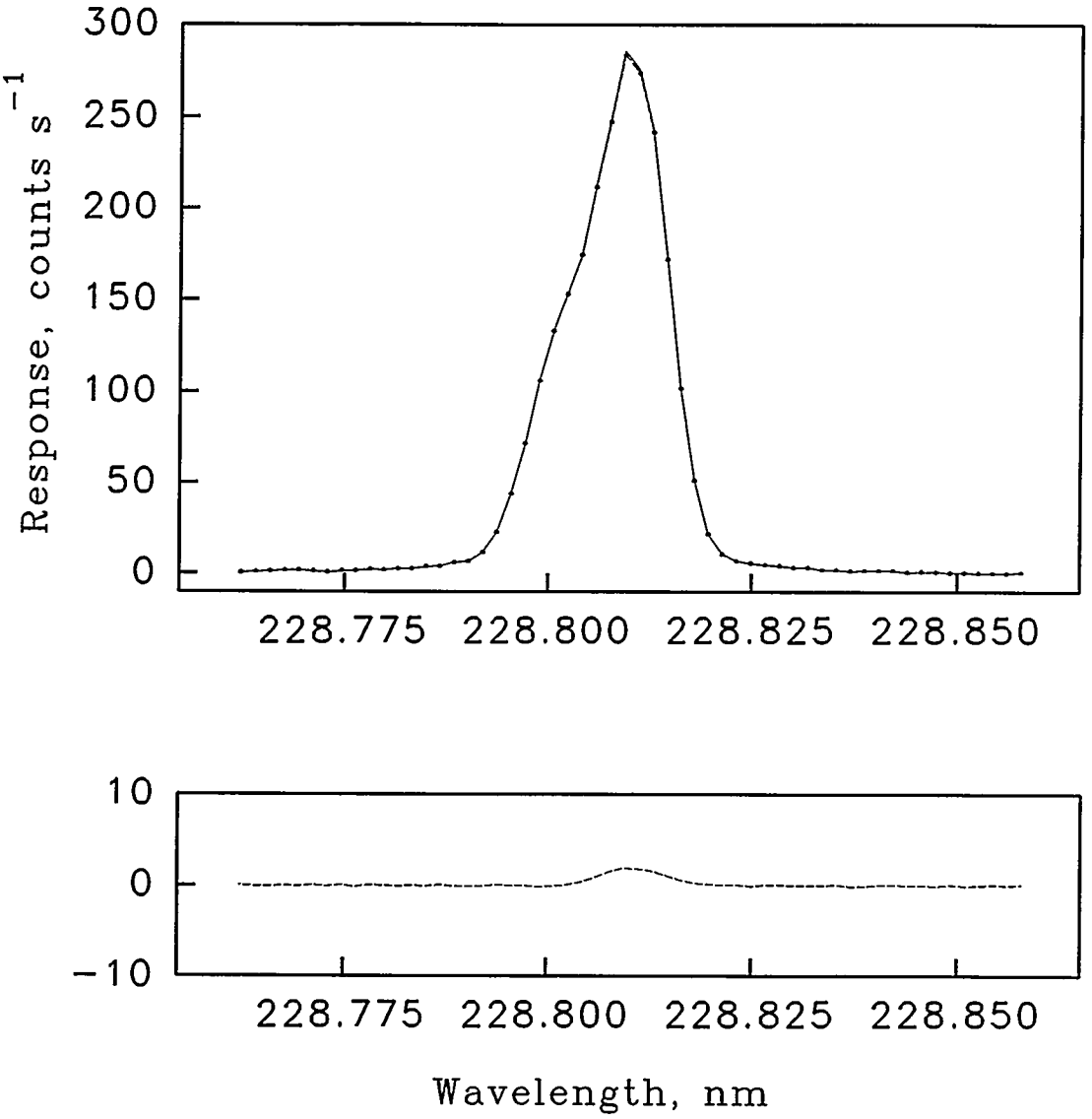

Fig. 3. Comparison of the experimental spectrum for the original sample solution (solid line) with the reconstructed spectrum based on GSAM calculation (filled circles). The spectrum at the bottom is the residuals vector (dash line) with the expanded vertical scale.

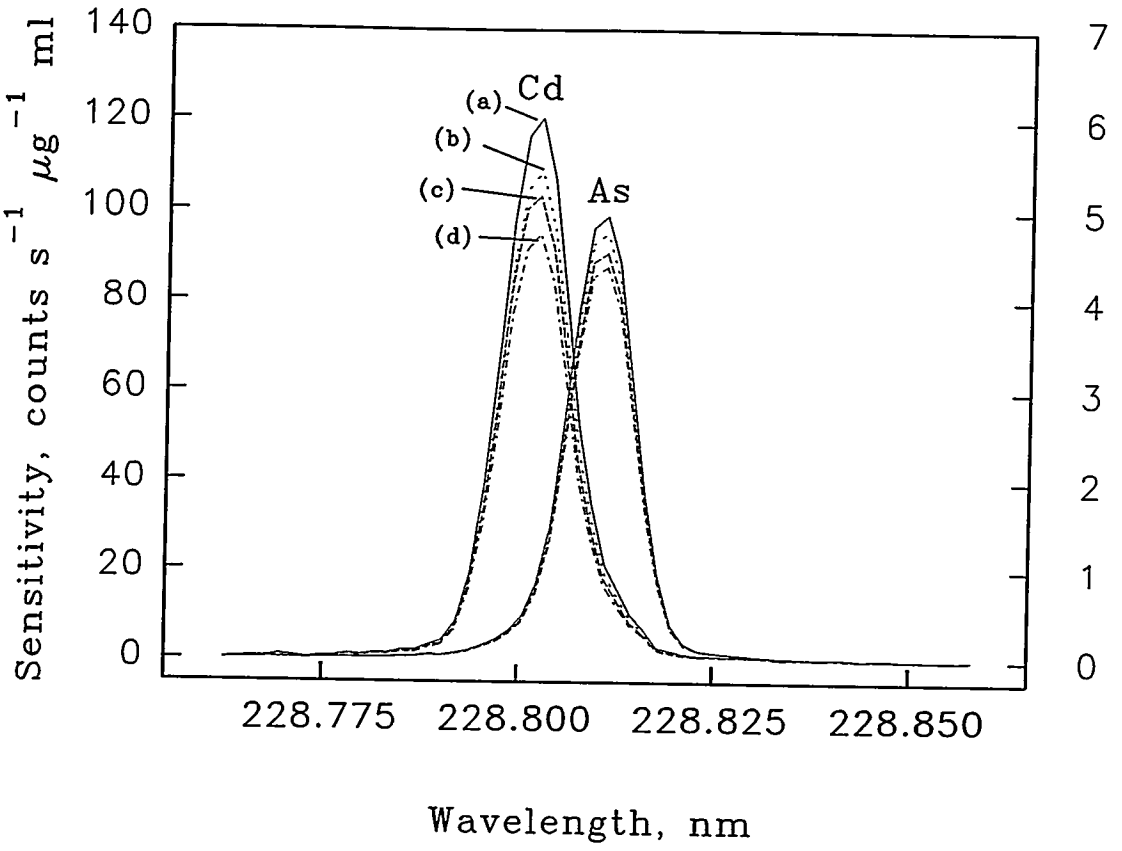

Fig. 4. The spectra of Cd and As extracted from the GSAM calculation obtained from

(a) 1.000 μg mℓ^{-1} Cd + 55.00 μg mℓ^{-1} As (solid line);

(b) 1.000 μg mℓ^{-1} Cd + 55.00 μg mℓ^{-1} As + 1000 μg mℓ^{-1} Na (dot line);

(c) 1.000 μg mℓ^{-1} Cd + 55.00 μg mℓ^{-1} As + 2000 μg mℓ^{-1} Na (dash line); and

(d) 1.000 μg mℓ^{-1} Cd + 55.00 μg mℓ^{-1} As + 3000 μg mℓ^{-1} Na (dash-dot line).

CHAPTER 4. OPTICAL EMISSION STUDIES OF THE MACH DISK EXTRACTED FROM AN INDUCTIVELY COUPLED PLASMA WITH AN ECHELLE SPECTROMETER AND SEGMENTED-ARRAY CHARGE-COUPLED DETECTORS[1]

A paper submitted to the Journal of Analytical Atomic Spectrometry

Shen Luan, Ho-ming Pang, and R. S. Houk[2]

Abstract

An inductively coupled plasma (ICP) is extracted into a small quartz vacuum chamber through a sampling orifice in a water-cooled copper plate. Optical emission from the Mach disk region is measured with a new type of echelle spectrometer equipped with two segmented-array charge-coupled-device detectors, the Optima 3000 from Perkin-Elmer. This device provides excellent quantum efficiency throughout the ultraviolet-visible region, as well as low dark current and readout noise. The spectral background emitted by the Mach disk is very low. Axial profiles of the optical emission of various atom and ion lines are measured. The effects of aerosol gas flow rate on the

---

[1] Presented at the Twenty-First Annual Conference of the Federation of Analytical Chemistry and Spectroscopy Societies (FACSS), St. Louis, Missouri, USA, October 2-7, 1994.

[2] To whom correspondence should be addressed.

intensities of various lines are investigated. The relationship between the location of the Mach disk and the pressure in the expansion chamber is also studied. The analyte line intensities are enhanced at higher pressure.

Keywords: *Inductively coupled plasma; supersonic jet; Mach disk; atomic emission spectrometry; simultaneous multielement analysis*

Introduction

Measurements of optical emission from the reduced-pressure plasma extracted from an atmospheric pressure inductively coupled plasma (ICP) were first demonstrated by Houk and Lim[1]. The analyte line intensities from the reduced-pressure plasma were weaker than those from the ICP by a factor of approximately 1000. However, the spectral background emitted by the reduced-pressure plasma was so low that it was indistinguishable from the dark current of the photomultiplier used (0.3 nA in this case). In contrast, a substantial background is seen from the ICP alone throughout the ultraviolet (UV)-visible region[2]. In a second paper by Lim *et al.*[3] some fundamental characteristics of the reduced-pressure plasma extracted from an ICP were described. Gas kinetic temperatures were measured in the Mach disk region of the extracted plasma from the widths of emission and fluorescence lines and from the intensities of various OH band components. These temperature values were in the range of 2200-2500 K, as expected if collisions in the Mach disk reheat the sampled gas to temperatures roughly half of those outside the sampler in the ICP[4,5].

Several others have also studied reduced-pressure emission sources extracted from ICPs. Kawaguchi *et al.*[6] measured the dependence of emission on spatial position and background pressure in the expansion chamber. Gray[7] reported a qualitative photographic study of the supersonic jet and shock waves. The expansion shrank and the Mach disk and barrel shock emitted more strongly as background pressure increased. Borer and Hieftje[8-10] evaluated the performance of a microwave-boosted reduced-pressure plasma extracted from an atmospheric pressure ICP. The reduced-pressure plasma was viewed axially, so that emission from the ICP outside the sampler was also collected, in contrast to the perpendicular viewing discussed in ref. 1. Shibata *et al.*[11] measured Ar (I) and H_β emission lines from the supersonic jet to determine electron density and excitation temperature.

Recently an echelle polychromator equipped with two segmented-array charge-coupled-device detectors (SCD) has been designed for inductively coupled plasma atomic emission spectrometry (ICP-AES)[12, 13]. This device provides high quantum efficiency in the UV region, low dark current, low readout noise, as well as simultaneous multielement capabilities, which are perfectly suited to a tandem emission source with a low spectral background. Our main objective was to evaluate the joint use of the Mach disk emission source extracted from an ICP with an echelle spectrometer equipped with SCDs.

Experimental

Extraction System

A scale diagram of the ICP and extraction system is shown in Fig. 1. The ICP torch along with the 40-MHz free-running radio-frequency (RF) generator from the Perkin-Elmer Optima 3000 were used here. The outer tube of the torch was shortened by 10 mm. The ICP was operated vertically. A cross-flow nebulizer and Scott-type, double-pass spray chamber were used to introduce aqueous samples. Typical operating conditions are listed in Table 1.

A circular sampling orifice was drilled in a copper sampling disk. Different orifice diameters ranging from 0.56 mm to 1.06 mm were tested in this work. The sampling disk (B in Fig. 1) was made very thin (approximately 4 mm in thickness), because it was considered desirable to be able to collect optical radiation from as close to the sampling orifice as possible. Soft copper tubing with an outside diameter of 3.2 mm was silver-soldered to the edge of the disk for water cooling. A shallow cone was made on the ICP side of the disk to make it easier to center the sampling orifice on the axial channel of the ICP. A quartz cylinder was used as the wall of the extraction chamber so that the extracted plasma could be measured optically in the UV region. Flat Viton gaskets (0.8 mm in thickness) and threaded retaining rods sealed the quartz cylinder to the sampling disk and pumping flange. A rotary vacuum pump (Edwards, E2M18, pumping speed of 5.7 l s^{-1}) was connected to the extraction system. A Convectron vacuum gauge (Granville-Phillips) was introduced into the vacuum line. The meter readings of the

gauge, which was factory-calibrated for nitrogen, were converted into argon pressures by using the conversion curve supplied by the manufacturer. An inline valve was also employed to control the pressure in the extraction chamber.

The entire extraction system was attached to a vertically movable stand which was fixed on top of the ICP torch box. The sampling orifice was centered on the ICP and was positioned 15 mm above the top of the load coil. The ICP was ignited with the sampling disk in position. The sampling disk was grounded. No severe secondary discharge or pinch effect[14, 15] was observed outside the sampling orifice. The orifice did not erode or expand over a period of several months, and Cu lines from the sampler were not observed.

Spectrometer

An echelle polychromator with an SCD detection system[12, 13] was used to measure the optical emission from the extracted plasma. Care was taken to shield the strong radiation from the ICP by using baffles made of steel sheets. The baffles were treated chemically to achieve a dull-black finish to intercept reflected and scattered light. The ceramic purge extension along with the quartz window was removed to accommodate the extraction system in the sample compartment. The vertical viewing position (viewing height) and the horizontal viewing position were changed by computer-controlled movement of the first transfer mirror. The viewing height could be changed from the load coil to 30 mm above the load coil in 1-mm increments. However, some astigmatism (5 mm)[12] was introduced in the vertical direction by the transfer optics.

In other words, a 5-mm high segment of the source was actually viewed by the spectrometer at each observation position. The horizontal viewing position could be adjusted from -10.0 to 10.0 mm in 0.4-mm increments.

Results and Discussion

Physical Appearance and Structure of Extracted Plasma

The physical appearance of the extracted plasma is depicted in Figs. 1 and 2. The dark "zone of silence" was clearly visible. The zone of silence was surrounded by a concentric barrel shock and terminated in a perpendicular shock wave called the Mach disk. These shock waves were characterized by faint, bluish red emission. Downstream from these shocks, a red afterglow continued for some distance[1, 6, 7].

Location of the Mach Disk as a Function of the Background Pressure in the Extraction Chamber

In his photographic study of the shock waves, Gray[7] shows that the shock envelope is more compact when the background pressure in the extraction chamber increases. Ashkenas and Sherman[16], in their supersonic molecular beam experiments, demonstrate that the Mach disk forms at a distance X_M from the orifice (Fig. 2) given by the following equation:

$$X_M/D = 0.67\ (P_0/P_1)^{1/2} \quad \ldots\ldots\ldots\ldots\ldots\ldots \quad (1)$$

where P_1 is the background pressure in the extraction chamber, P_0 is the source pressure (740.1 torr in this case), and D is the orifice diameter. The validity of eqn. (1) for high temperature, partially ionized gases, such as the ICP, has been confirmed by Kawaguchi *et al.*[6]

In this present study, the location of the onset of the Mach disk X_M (Fig. 2) is measured by a cathetometer, which consists of a telescopic leveling apparatus that slides up and down on a perpendicular stand with a finely graduated scale. The resolution of the scale for the cathetometer used is 0.05 mm. A log-log plot of X_M/D *vs.* P_0/P_1 is shown in Fig. 3. Results of linear regression are also shown in Fig. 3, with a R value or correlation coefficient of 0.998.

The change in location of the Mach disk with varying background pressure conforms closely to that predicted from eqn. (1)[16] obtained in supersonic molecular beam experiments. The rather small difference between the coefficient found in this work and that from eqn. (1) (*i.e.*, 0.62 *vs.* 0.67) is probably due to the difference between the pressure measured by the gauge and the true ambient pressure in the chamber. The range of the measured background pressure was fairly narrow in this study (from 1.8 to 9.5 torr). The shock envelope was very faint at lower pressure, making the measurement of the exact location of the onset of the Mach disk very difficult. On the other hand, at higher pressures the shock envelope became more compact and was eventually blocked by the thin sampling disk.

Axial Emission Profiles

Axial profiles of the optical emission of various atom (I) and ion (II) lines are shown in Fig. 4. In this study, the viewing height was changed by computer control of the image transfer optics. In these profiles, the horizontal coordinate is distance from the orifice (instead of viewing height above the top of the load coil). The sampling orifice is 15 mm above the top of the load coil. The orifice used here was 0.56 mm diameter[1], and the argon pressure in the extraction chamber was 1.8 torr while sampling the ICP.

As can be seen from Fig. 4, the intensities in the "zone of silence" are low. They increase drastically with increasing distance from the orifice and reach maxima at around 7 mm from the orifice, which corresponds to the location of the Mach disk. For neutral atom lines (I), the profiles level off or drop off slightly above the location of the Mach disk, while for ion lines (II), the profiles drop off much more significantly. The difference between the profiles for atom (I) and ion (II) lines is more profound for Mg than for analogous lines from Ca or Sr.

Effect of Aerosol Gas Flow Rate on Emission

The dependence of analyte line intensity on aerosol gas flow rate is shown in Fig. 5. In this study, the viewing height was chosen to be 7 mm above the orifice (22 mm above top of the load coil). The neutral atom lines (I) peaked at around 1.4-1.6 l min^{-1}. However, for ion lines (II), some interesting features appear. The intensities of the Mg (II) lines are maximum at 0.6-0.7 l min^{-1}. The profiles for Ca (II) lines are double-humped, with one peak at 0.7-0.8 l min^{-1} and a second one at

1.6 l min^{-1}. For Sr (II) lines, the maxima are at 1.6-1.7 l min^{-1}, with another small hump at about 0.8 l min^{-1}.

In principle the ionic emission from the Mach disk $I_{M^+, MD}$ can be expressed by the following proportionality:

$$I_{M^+, MD} \propto n_{M^+, MD} \times e^{-E^*/k T_{exc, MD}} \quad \ldots\ldots\ldots\ldots \quad (2)$$

where $n_{M^+, MD}$ is the number density of M^+ ions in the Mach disk, E^* is the excitation energy of M^+ ions, k is Boltzmann's constant, and $T_{exc, MD}$ is the excitation temperature in the Mach disk. The terms $n_{M^+, MD}$ and $T_{exc, MD}$ in eqn. (2) are proportional to the analogous quantities outside the sampler in the ICP:

$$n_{M^+, MD} \propto n_{M^+, ICP} \quad \ldots\ldots\ldots\ldots\ldots\ldots \quad (3)$$

$$T_{exc, MD} \propto T_{exc, ICP} \quad \ldots\ldots\ldots\ldots\ldots\ldots \quad (4)$$

where $n_{M^+, ICP}$ and $T_{exc, ICP}$ are number density of M^+ ions and excitation temperature of the ICP just outside of the sampling orifice.

When the aerosol gas flow rate is set to 1.6 l min^{-1}, the apex of the initial radiation zone[17] formed by aspirating an yttrium solution at 1000 μg ml^{-1} is located about 1-2 mm below the sampling orifice. This sampling position generally corresponds to the highest M^+ signal in ICP mass spectrometry (ICP-MS)[18], hence the highest value of $n_{M^+, ICP}$ (hence $n_{M^+, MD}$) is obtained here. This ion number density factor is most important when a relatively small orifice (0.56 mm diameter in this case) is used, because only the center part of the axial channel is sampled. However, at lower aerosol gas flow rate (0.7 l min^{-1}), the sampling position is in the middle of the normal analytical zone[17], which is the region where $T_{exc, ICP}$ (hence $T_{exc, MD}$) is highest.

Thus, the variation of ion line intensity with aerosol gas flow rate is caused by a competition between the $n_{M^+,MD}$ factor and the Boltzmann factor in eqn. (2). For high E^* lines (such as Mg (II) 279.553 nm and Mg (II) 280.270 nm), the Boltzmann factor is more important. Therefore, Mg (II) emission is a maximum at lower aerosol gas flow rate. For low E^* lines (such as Sr (II) 407.771 nm and Sr (II) 421.552 nm), the $n_{M^+,MD}$ factor is more important, so they peak at higher aerosol gas flow rate. The double emission humps for Ca (II) 393.366 nm and Ca (II) 396.847 nm indicate that the spatial changes in the ion number density factor and Boltzmann factor are of similar magnitude in this case.

Effects of Background Pressure and Orifice Diameter

With the orifice diameter of 0.56 mm and background pressure in the extraction chamber of 1.8 torr, the spectral background emitted by the Mach disk is very low, usually less than 0.1 counts s^{-1} for 200 seconds integration time. However, it is obvious that the analyte intensities from the Mach disk need to be enhanced.

One simple way to boost the analyte intensities from the Mach disk is to increase background pressure in the extraction chamber[6, 7]. Looking at eqn. (1), when P_1 increases, X_M becomes shorter. If the Mach disk is too close to the orifice, optical emission from the Mach disk will be difficult to measure, simply because it will be blocked by the sampling disk. Looking more closely at eqn. (1), if D increases, X_M becomes longer. In this study, the orifice diameter was then enlarged to 1.06 mm and the background pressure was increased to 9.5 torr.

At a background pressure of 9.5 torr, the flow pattern downstream of the Mach disk is different from the case of 1.8 torr, as shown in Fig. 6. With higher background pressure, the reflected shock forms a second barrel and another disk. Increasing the background pressure even further, the pattern is repeated along the axis many times. As many as five successive patterns are observed with background pressure around 20 torr. Similar observations have been made by Gray[7].

Axial profiles of the optical emission of various atom (I) and ion (II) lines with background pressure of 9.5 torr and orifice diameter of 1.06 mm are shown in Fig. 7. Generally speaking, the analyte line intensities are enhanced by using higher background pressure and larger orifice diameter. The axial profiles are maximized neither at the location of the Mach disk (7 mm) nor at the location of the second disk (14 mm). For the lines studied, a viewing height 12 mm above the orifice was chosen to be the optimum viewing position.

The effect of aerosol gas flow rate was also studied, as shown in Fig. 8. The most striking result is that most of the double-hump behavior is removed. The intensities of ion (II) lines are all maximized at around 0.7-0.9 l min^{-1}. When the orifice diameter was enlarged to 1.06 mm, all of the axial channel was sampled through the sampling orifice at all the aerosol gas flow rates studied[19]. Apparently, changes in the ion number density factor with aerosol gas flow rate became less significant, instead, the Boltzmann factor became dominant [eqn. (2)].

Detection Limits

Detection limits were measured for the most intense line for each element studied, as shown in Table 2. Operating conditions for these detection limits are as follows: orifice diameter 1.06 mm; background pressure 9.5 torr; viewing height 12 mm above the orifice; aerosol gas flow rate 0.8 l min^{-1}; integration time 200 s.

Detection limits in the range of 2-6 ng ml^{-1} were obtained. The intensities shown in Table 2 are still lower than those seen from the ICP by factors of 100 to 1000[21]. Obviously, the analyte signal from the Mach disk must be enhanced further. Several possible ways to implement such enhancements are currently under investigation in authors' laboratory, including backfilling the chamber with He, applying RF voltage to an electrode located at a position downstream from the Mach disk, and incorporating a magnetic mirror. Ideally these measures would enhance analyte signal more than background.

Acknowledgements

The authors gratefully acknowledge the Perkin-Elmer Corporation for the loan of the Optima 3000 atomic emission spectrometer. Ames Laboratory is operated by Iowa State University for the U.S. Department of Energy under contract No. W-7405-Eng-82. This research was supported by the Office of Basic Energy Sciences, Division of Chemical Sciences.

References

1. Houk, R. S., and Lim, H. B., *Anal. Chem.*, 1986, **58**, 3244.

2. Winge, R. K., Fassel, V. A., Peterson, V. J., and Floyd, M. A., *Inductively Coupled Plasma-Atomic Emission Spectroscopy. An Atlas of Spectral Information*, Elsevier, Amsterdam, 1985.

3. Lim, H. B., Houk, R. S., Edelson, M. C., and Carney, K. P., *J. Anal. At. Spectrom.*, 1989, **4**, 365.

4. Douglas, D. J., and French, J. B., *J. Anal. At. Spectrom.*, 1988, **3**, 743.

5. Fraser, R. B., Robben, F., and Talbot, L., *Phys. Fluids*, 1971, **14**, 2317.

6. Kawaguchi, H., Asada, K., and Mizuike, A., *Mikrochim. Acta*, 1988, **III**, 143.

7. Gray, A. L., *J. Anal. At. Spectrom.*, 1989, **4**, 371.

8. Borer, M. W., and Hieftje, G. M., *Spectrochim. Acta Rev.*, 1991, **14**, 463.

9. Borer, M. W., and Hieftje, G. M., *J. Anal. At. Spectrom.*, 1993, **8**, 333.

10. Borer, M. W., and Hieftje, G. M., *J. Anal. At. Spectrom.*, 1993, **8**, 339.

11. Shibata, N., Fudagawa, N., and Kubota, M., *Spectrochim. Acta, Part B*, 1992, **47**, 505.

12. Barnard, T. W., Crockett, M. I., Ivaldi, J. C., and Lundberg, P. L., *Anal. Chem.*, 1993, **65**, 1225.

13. Barnard, T. W., Crockett, M. I., Ivaldi, J. C., Lundberg, P. L., Yates, D. A., Levine, P. A., and Sauer, D. J., *Anal. Chem.*, 1993, **65**, 1231.

14. Houk, R. S., Fassel, V. A., Flesch, G. D., Svec, H. J., Gary, A. L., and Taylor, C. E., *Anal. Chem.*, 1980, **52**, 2283.

15. Houk, R. S., Fassel, V. A., and Svec, H. J., *Dynamic Mass Spectrom.*, 1981, **6**, 234.

16. Ashkenas, H., and Sherman, F. S., in *Rarefied Gas Dynamics, Proc. 4th Int. Symp. Rarefied Gas Dynamics*, ed. de Leeuw, J. H., Academic Press, New York, 1966, vol. II, pp. 84-105.

17. Koirtyohann, S. R., Jones, J. S., and Yates, D. A., *Anal. Chem.*, 1980, **52**, 1966.

18. Jarvis, K. E., Gray, A. L., and Houk, R. S., *Handbook of Inductively Coupled Plasma Mass Spectrometry*, Blackie, Glasgow, 1992.

19. Douglas, D. J., and French, J. B., *J. Anal. At. Spectrom.*, 1988, **3**, 743.

20. Ivaldi, J. C., and Barnard, T. W., *Spectrochim. Acta, Part B*, 1993, **48**, 1265.

21. Mermet, J. M., and Ivaldi, J. C., *J. Anal. At. Spectrom.*, 1993, **8**, 795.

Table 1. Typical instrumental operating conditions

Component	Operating conditions
RF generator	RF power: 1100 W
ICP torch	Plasma gas flow: 15 l min^{-1}
	Auxiliary gas flow: 1.0 l min^{-1}
Cross-flow nebulizer	Nebulizer gas flow: 1.000 l min^{-1}
	Liquid flow: 1.0 ml min^{-1}

Table 2. Detection limits

Element	Wavelength/ nm	Z_a*/ counts s^{-1}	Z_b†/ counts s^{-1}	σ‡/ counts s^{-1}	DL§/ ng ml^{-1}
Mg	279.553	41.8	0.20	0.081	6
Ca	393.366	98.2	0.16	0.072	2
Sr	407.771	51.2	0.19	0.077	4

Notation Z_a, Z_b, σ, and DL is from ref. 20.

* Z_a is the peak intensity of the analyte with background correction. The analyte concentration is 1000 ng ml^{-1}.

† Z_b is the net peak intensity of the spectral background at wavelength of peak maximum.

‡ σ is the standard deviation of the blank in the unit of counts per second.

§ DL is the 3 times the standard deviation of the blank in the concentration unit.

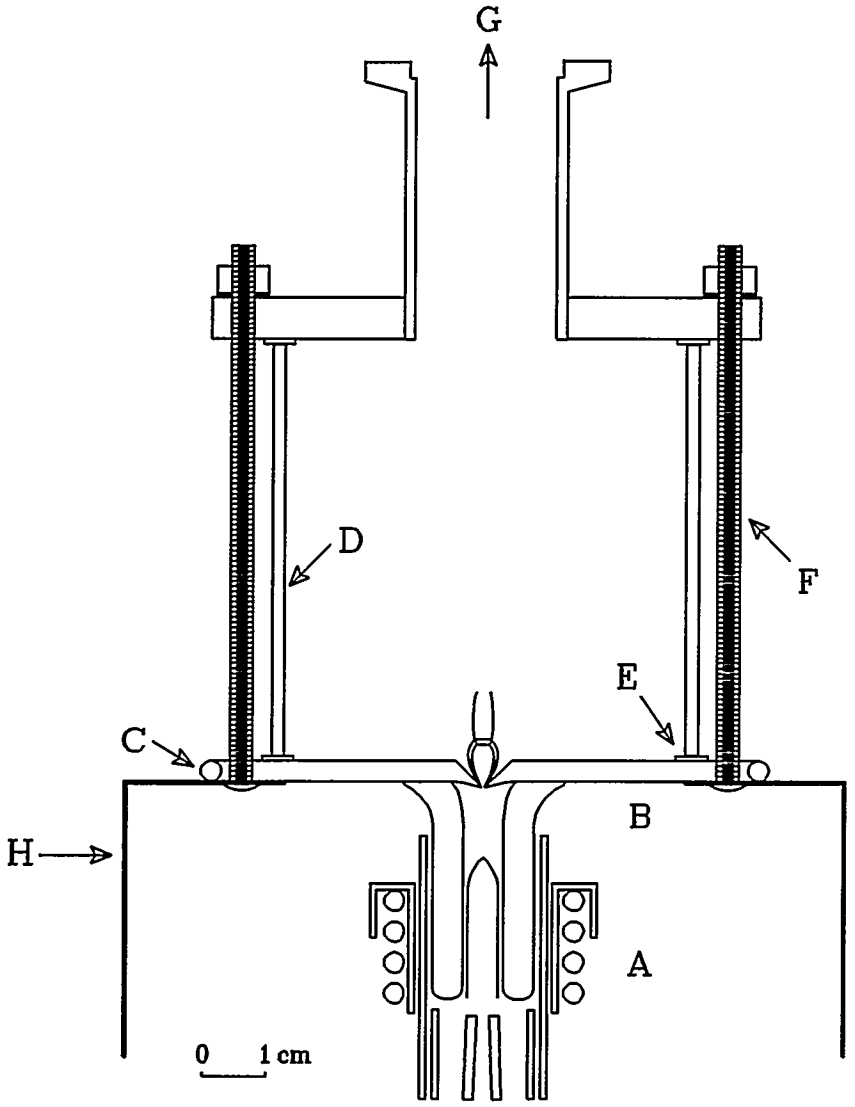

Fig. 1. ICP and extraction system. A: ICP torch, load coil, and bonnet; B: copper sampling disk; C: water cooling coil; D: cylindrical quartz tube; E: flat Viton gasket; F: threaded retaining rod; G: pumping port; and H: optical baffles.

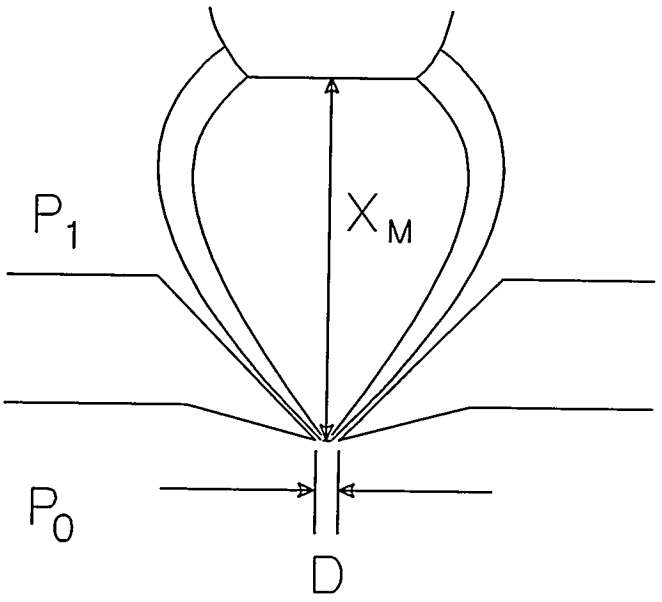

Fig. 2. Mach disk formation at a distance X_M from the orifice.

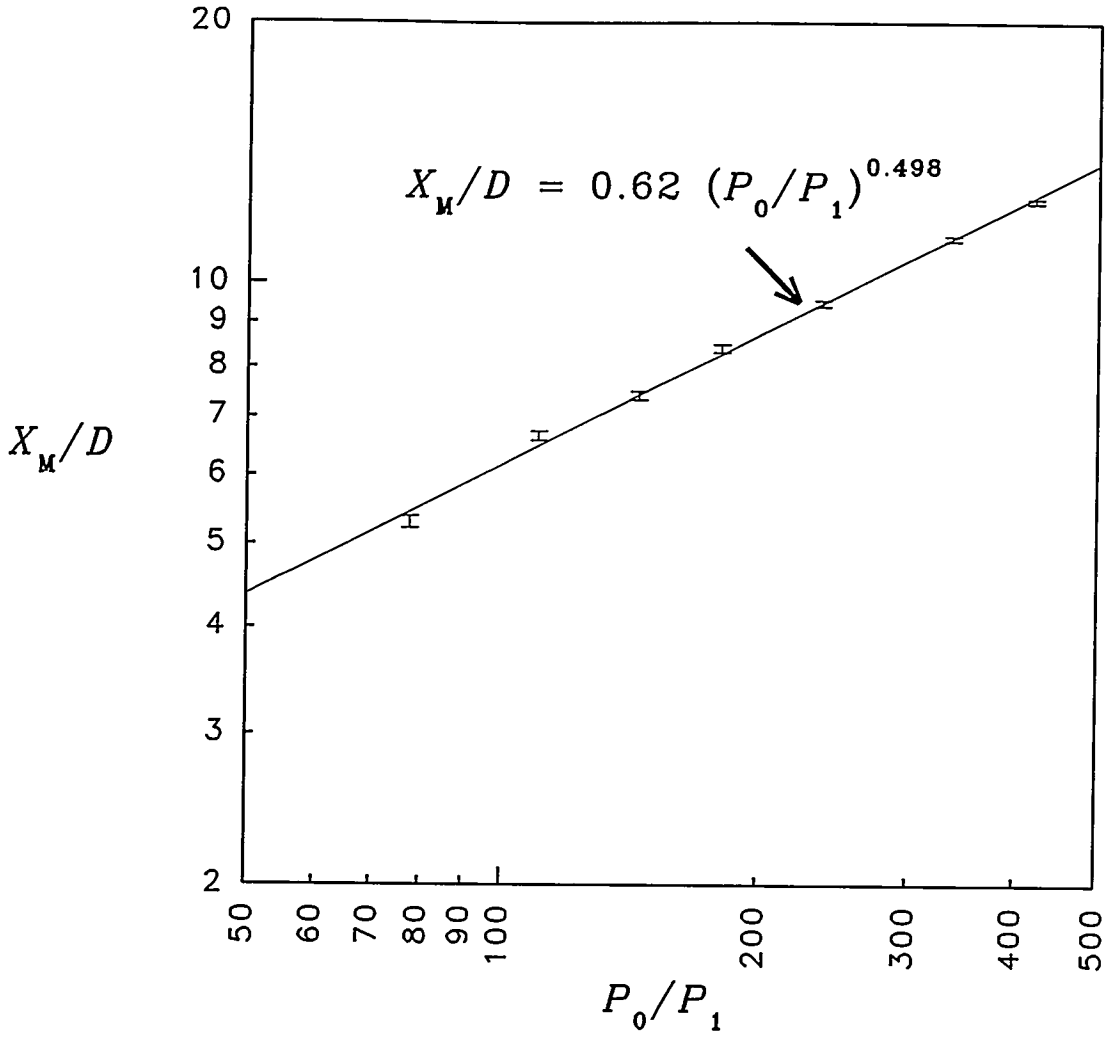

Fig. 3. Location of the Mach disk as a function of the argon background pressure in the extraction chamber (P_1). The orifice diameter (D) used here was 0.85 mm and atmospheric pressure (P_0) was 740.1 torr. Note the error bars for the X_M/D values.

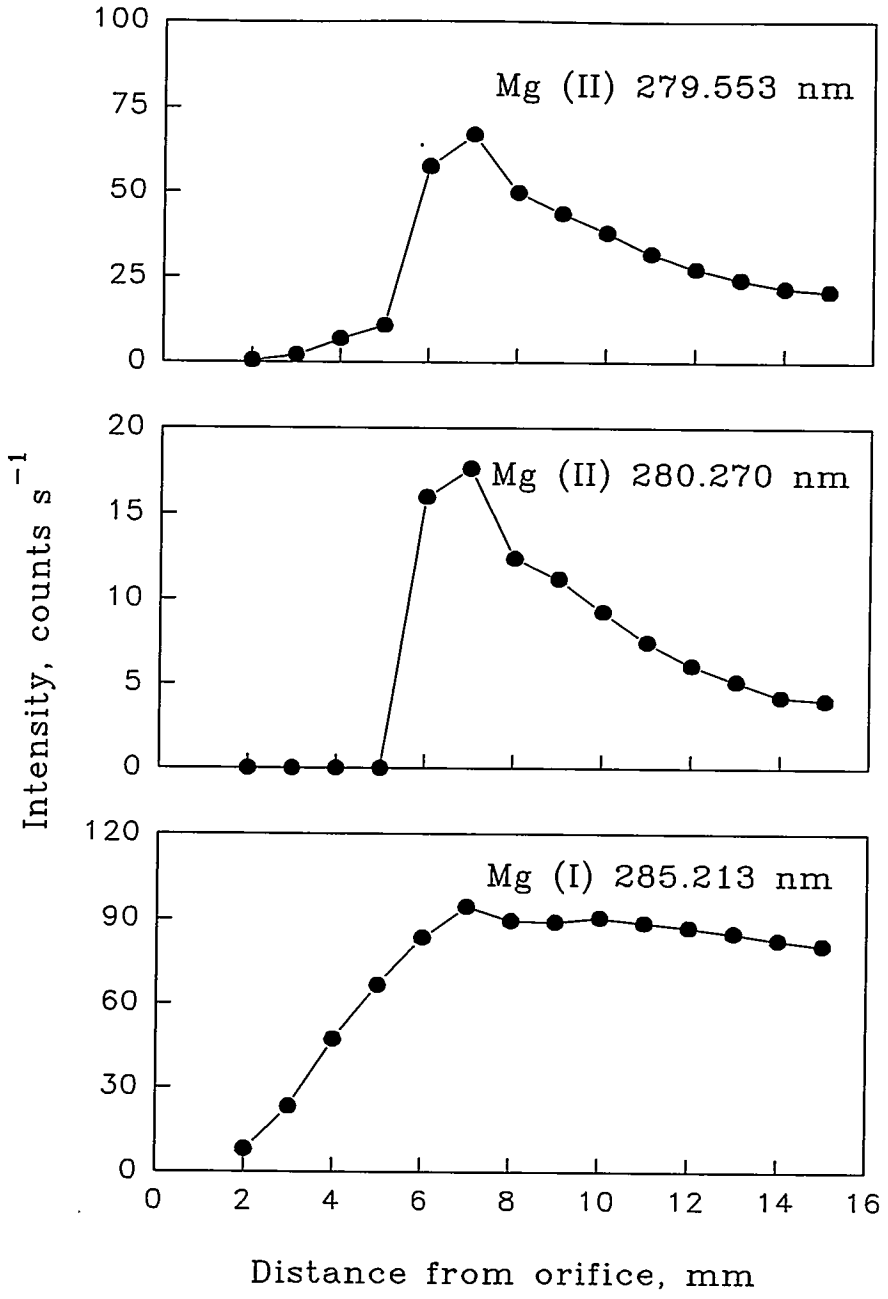

Fig. 4. Axial profiles of the optical emission of various atom (I) and ion (II) lines. The orifice used was 0.56 mm diameter. The background pressure in the extraction chamber was 1.8 torr. The concentrations of these elements were 50 μg ml^{-1}.

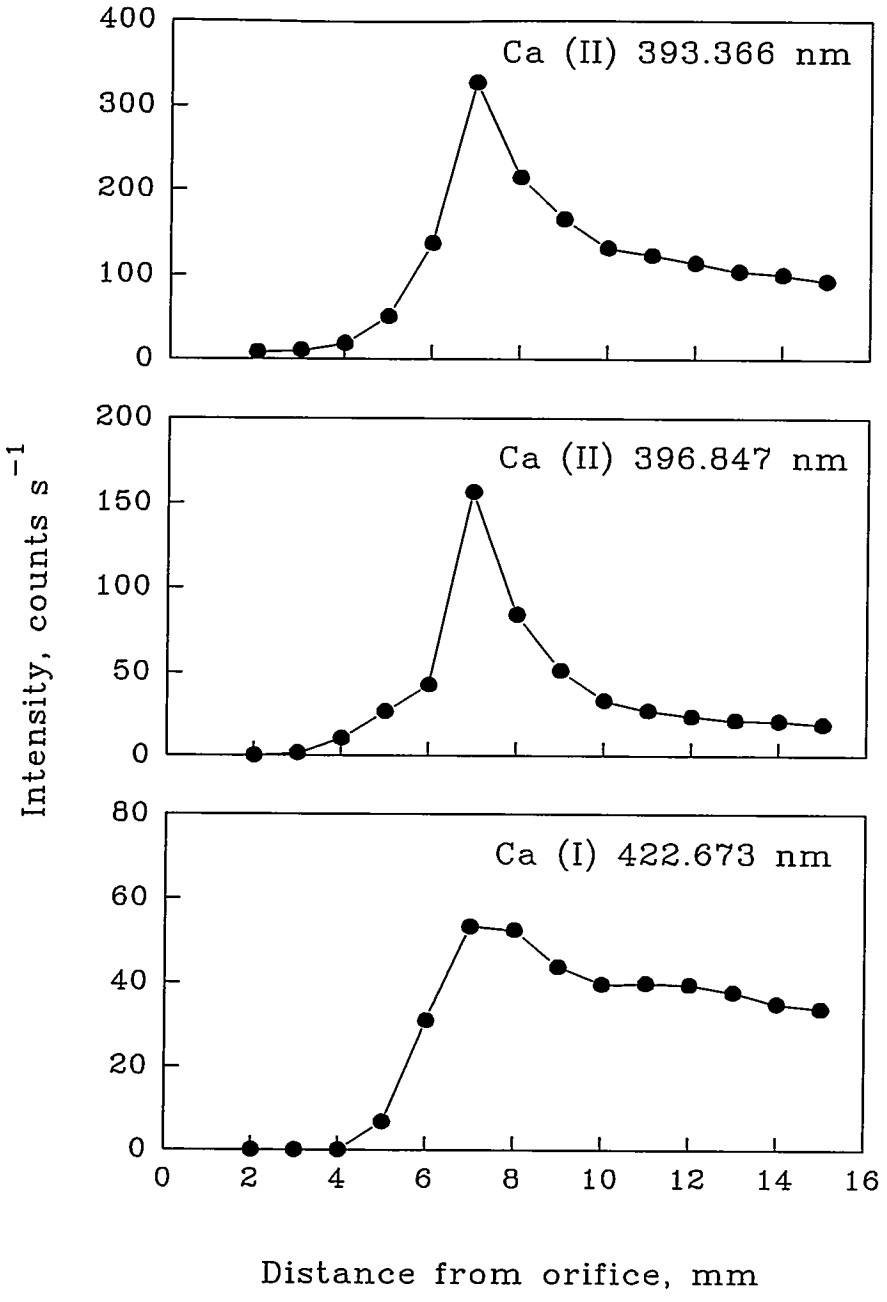

Fig. 4. (continued)

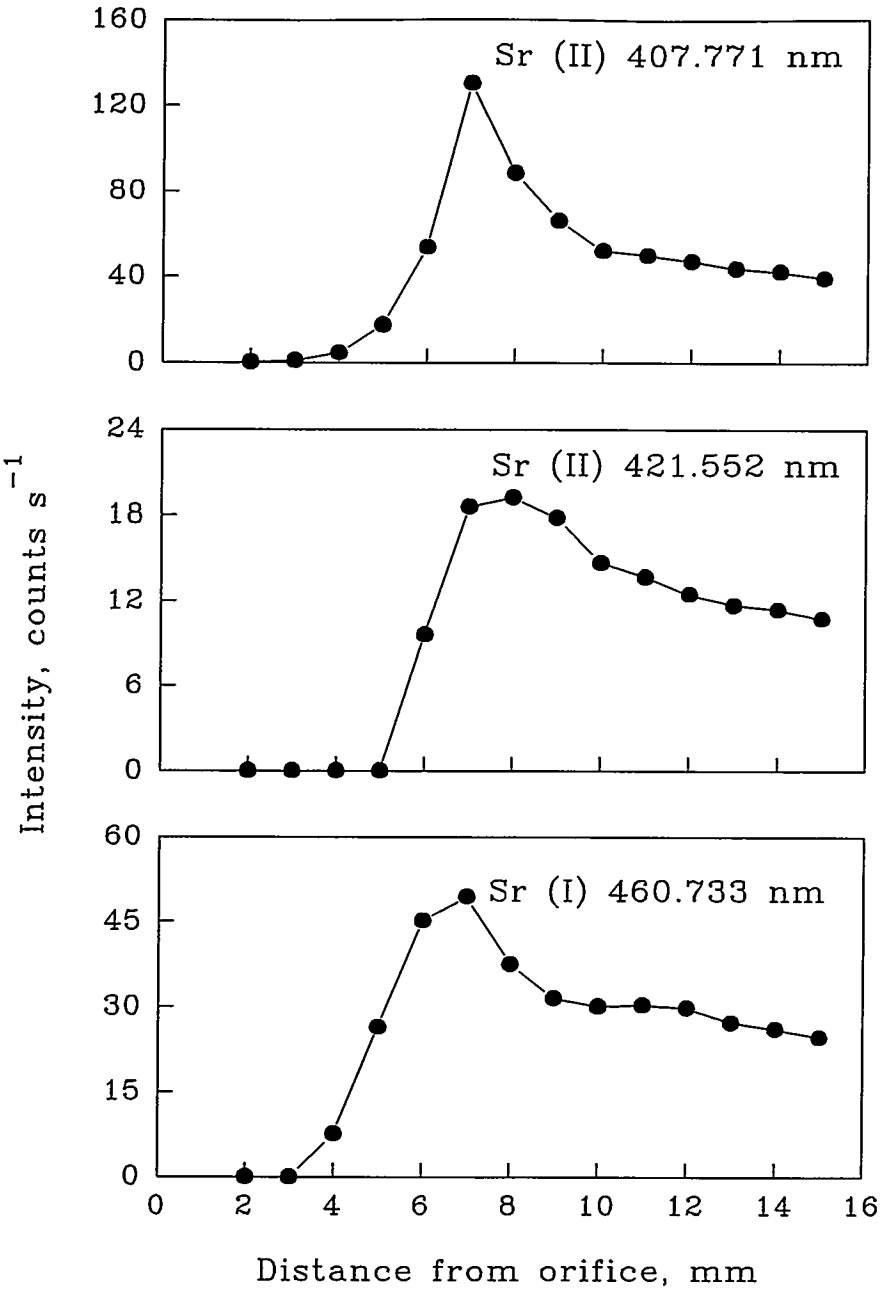

Fig. 4. (continued)

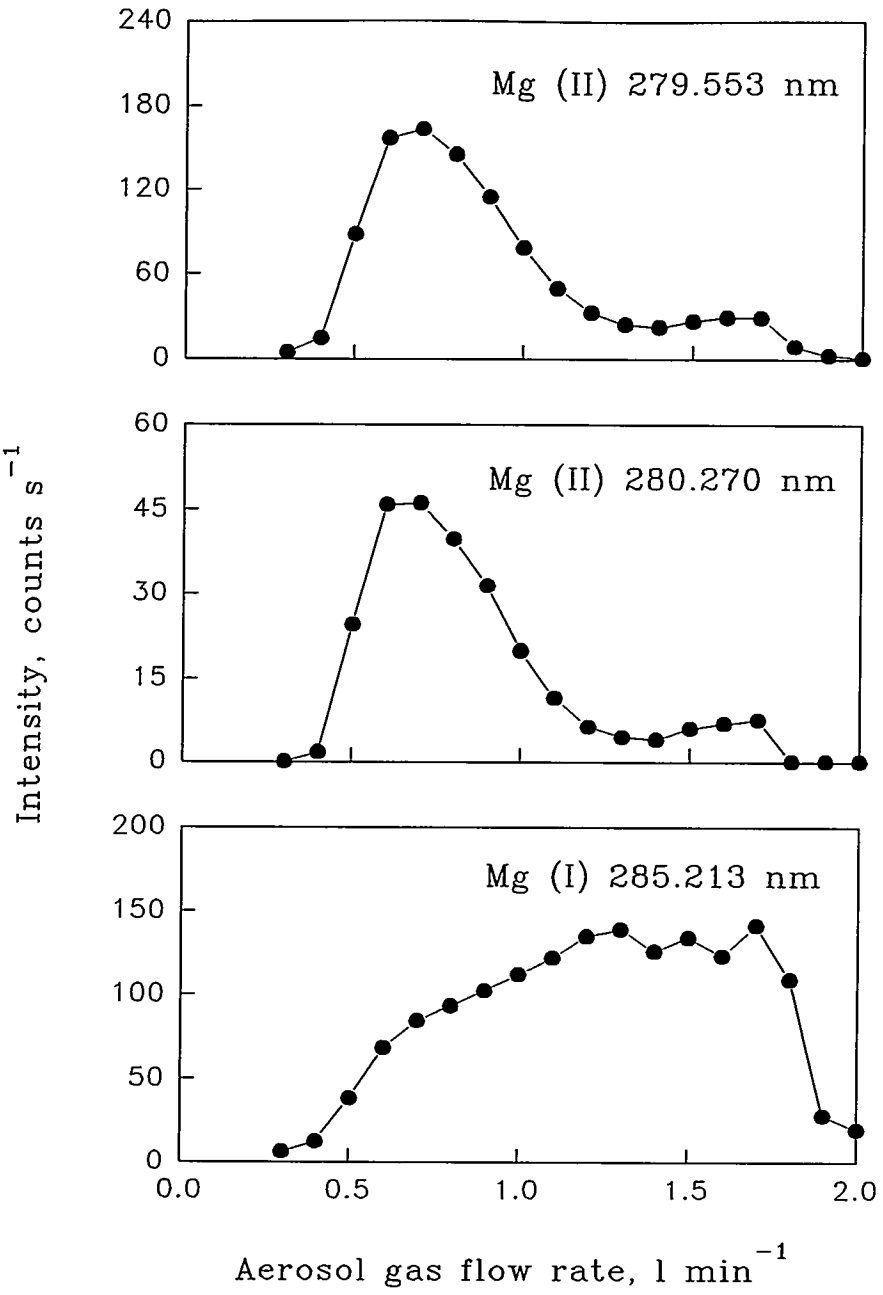

Fig. 5. Dependence of analyte line intensity on aerosol gas flow rate. The orifice used was 0.56 mm diameter. The background pressure in the extraction chamber was 1.8 torr. The concentrations of these elements were 50 μg ml^{-1}.

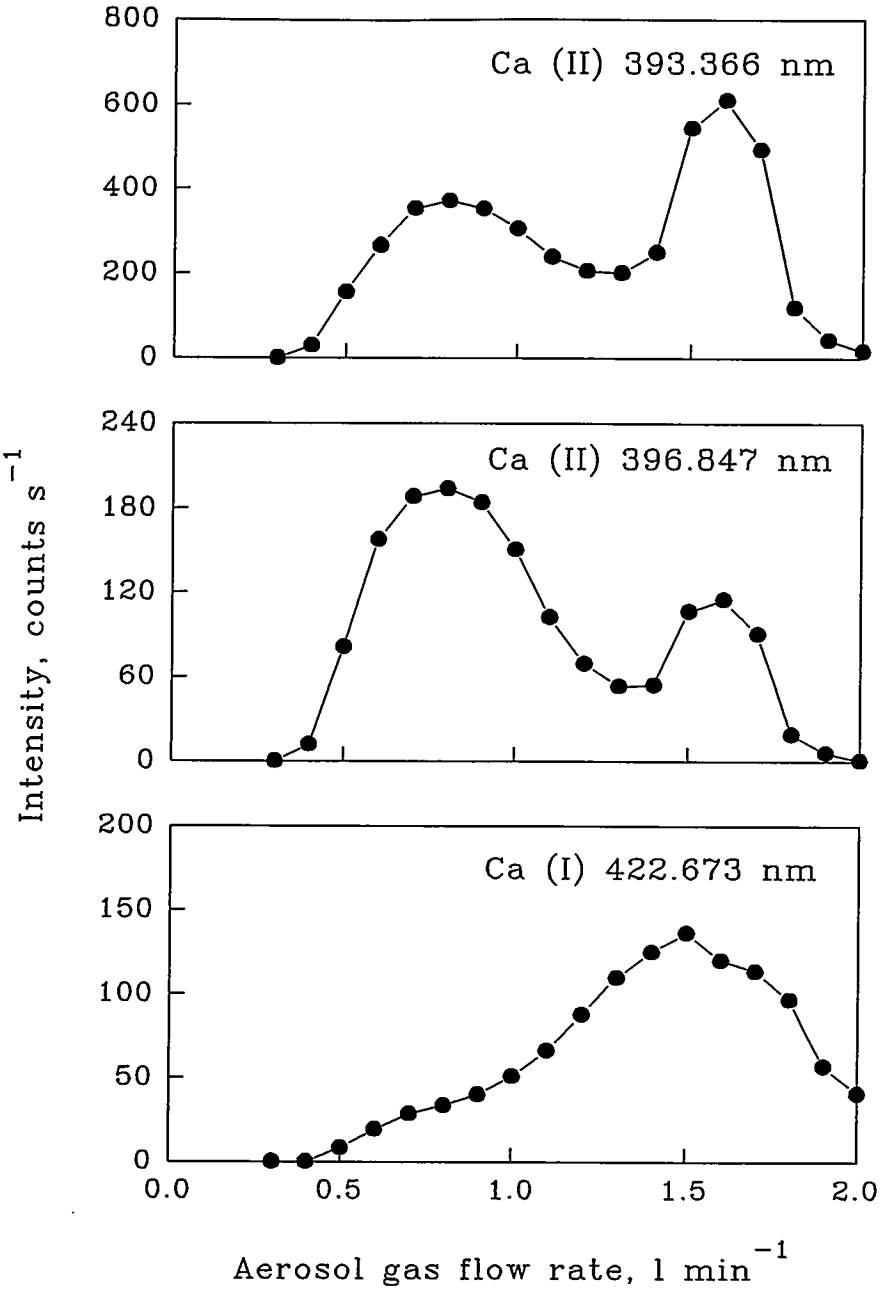

Fig. 5. (continued)

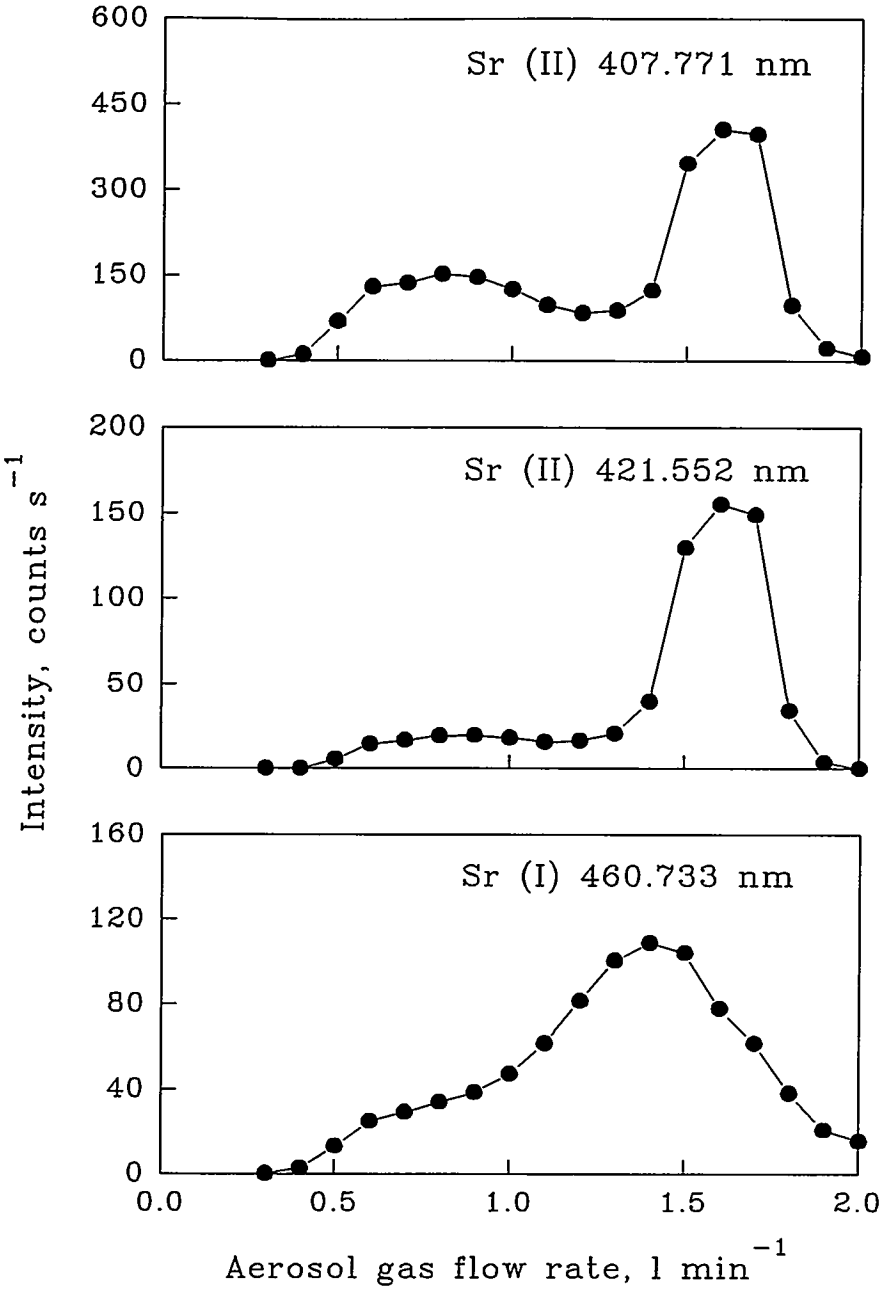

Fig. 5. (continued)

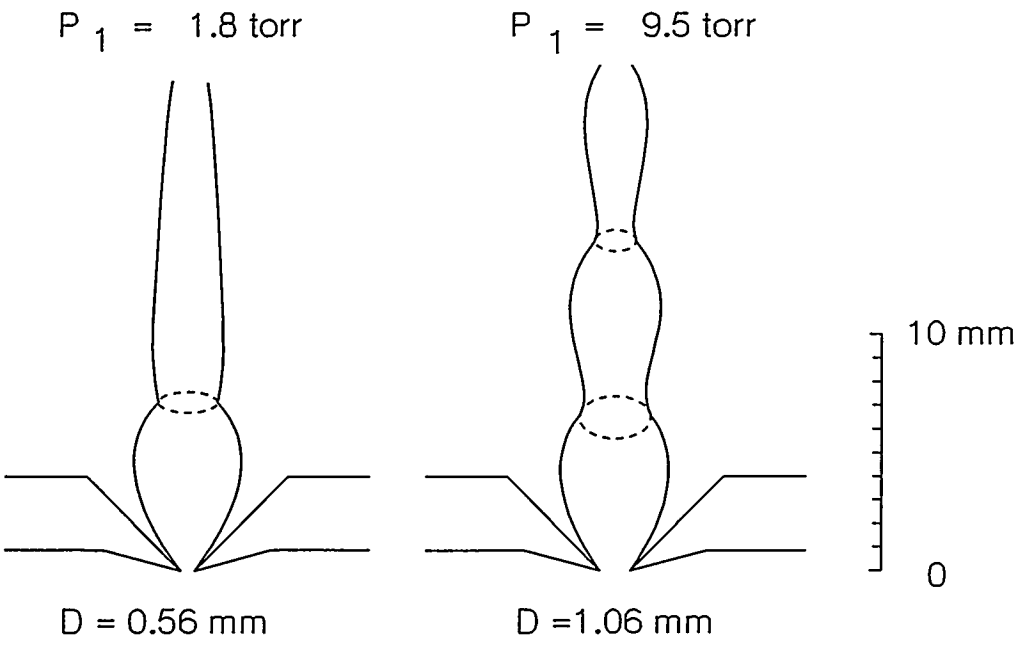

Fig. 6. Dependence of the structure of the extracted plasma on background pressure and orifice diameter.

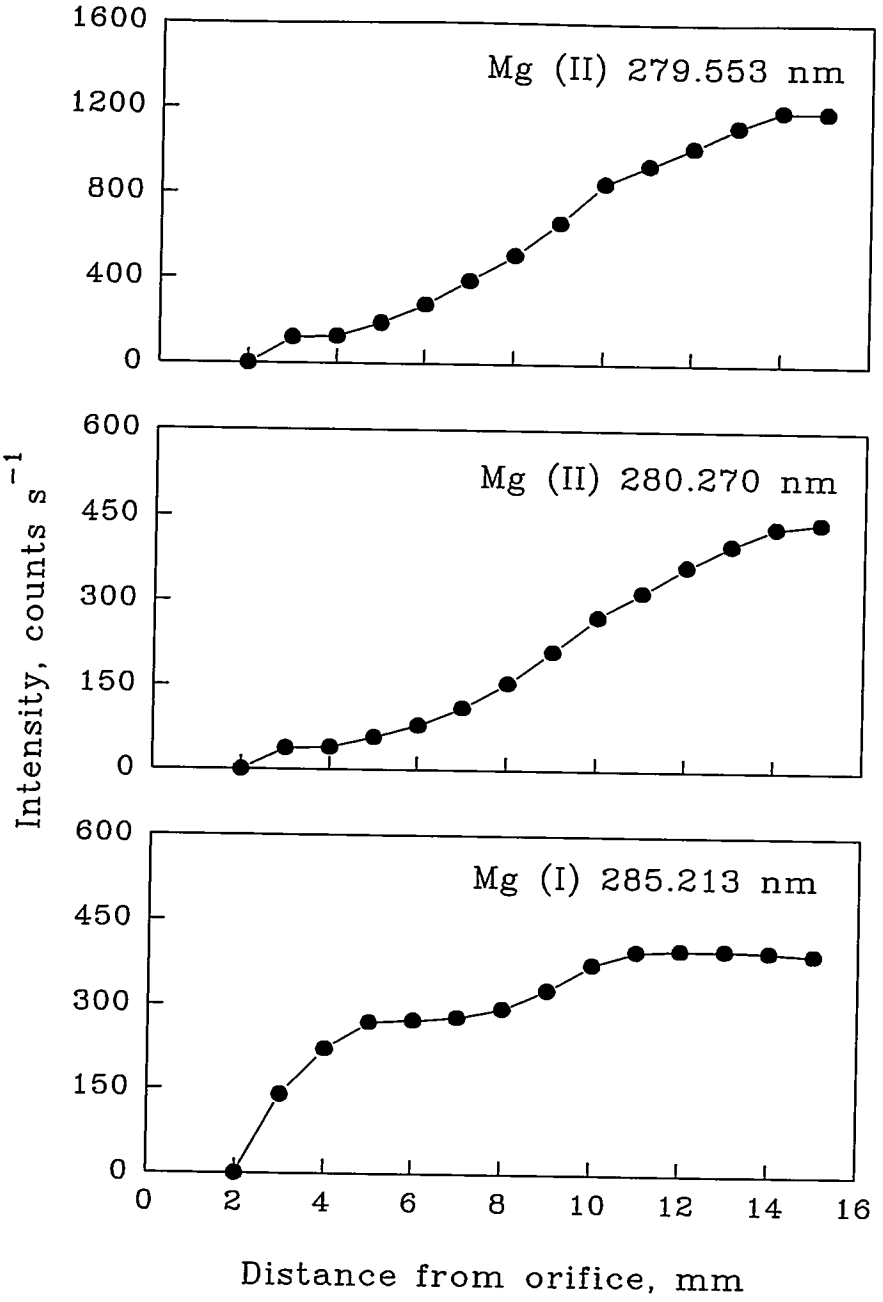

Fig. 7. Axial profiles of the optical emission of various atom (I) and ion (II) lines. The orifice used was 1.06 mm diameter. The background pressure in the extraction chamber was 9.5 torr. The concentrations of these elements were 50 μg ml^{-1}.

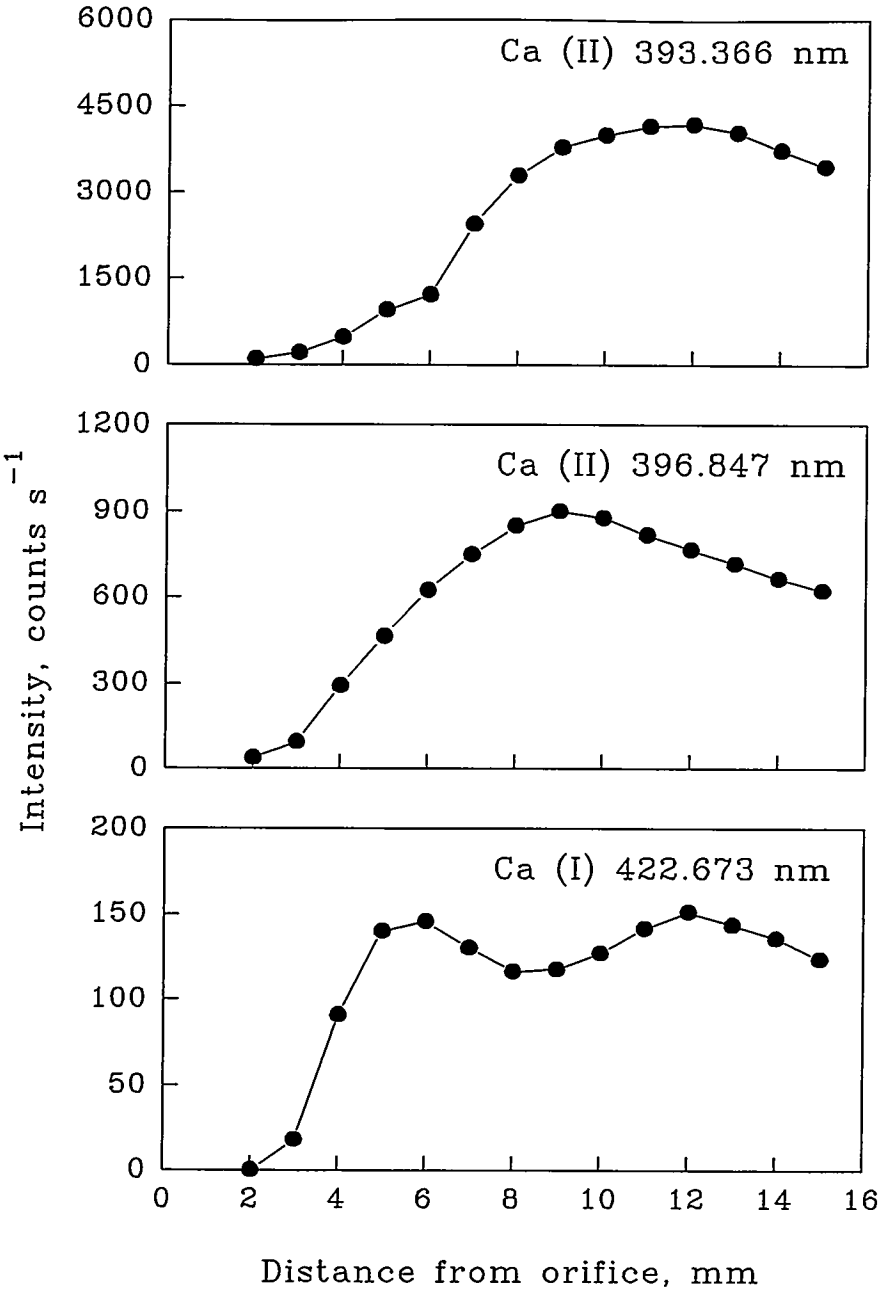

Fig. 7. (continued)

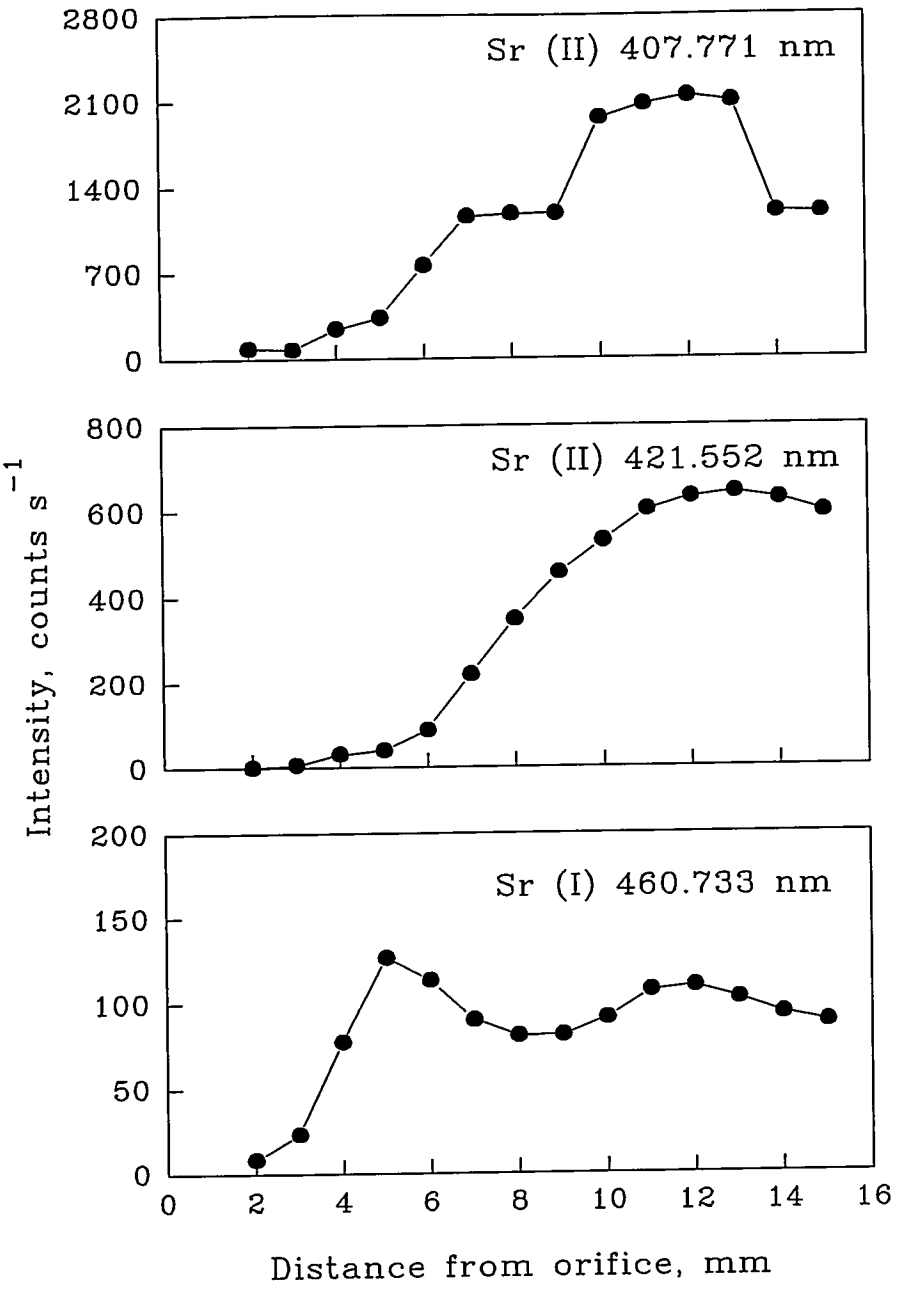

Fig. 7. (continued)

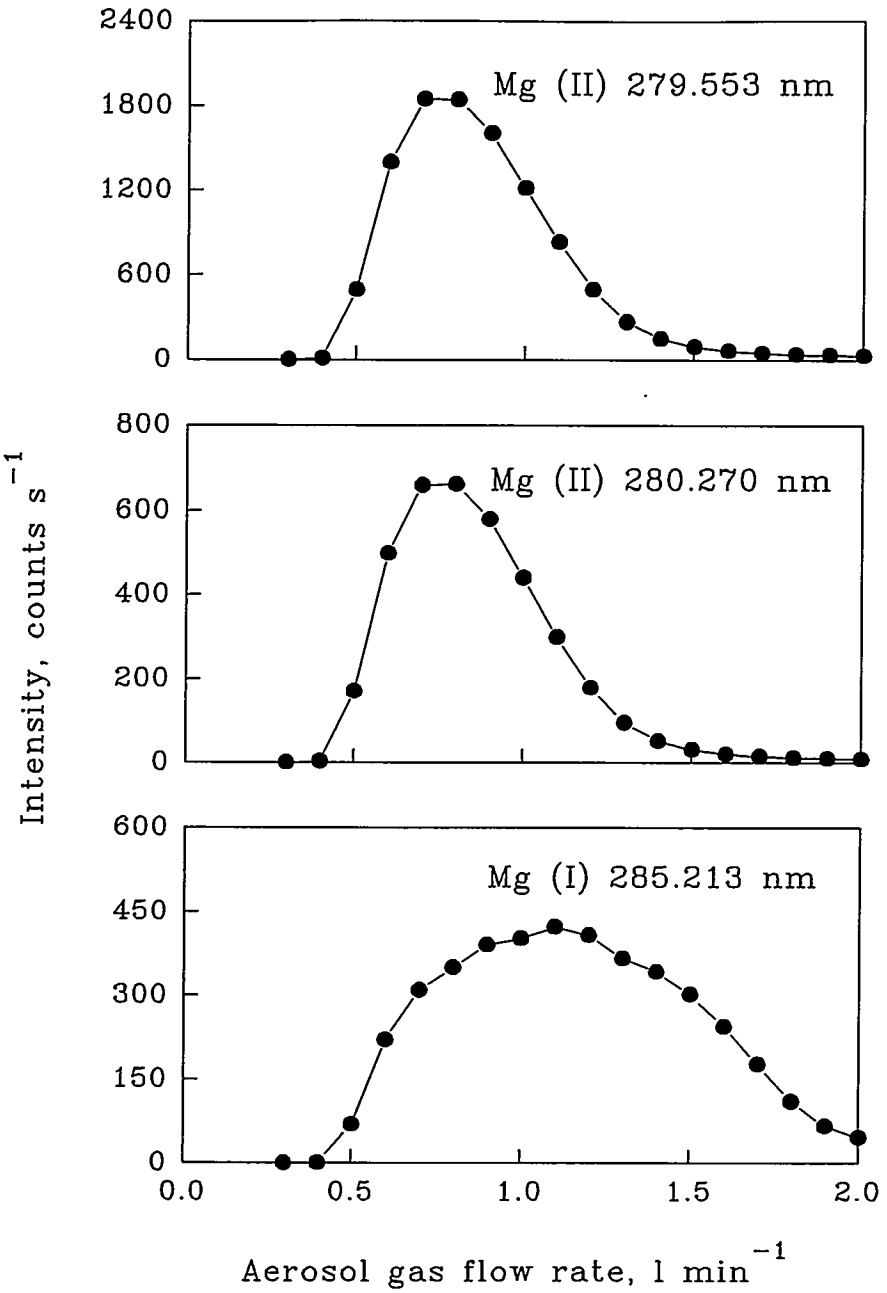

Fig. 8. Dependence of analyte line intensity on aerosol gas flow rate. The orifice used was 1.06 mm diameter. The background pressure in the extraction chamber was 9.5 torr. The concentrations of these elements were 50 μg ml^{-1}.

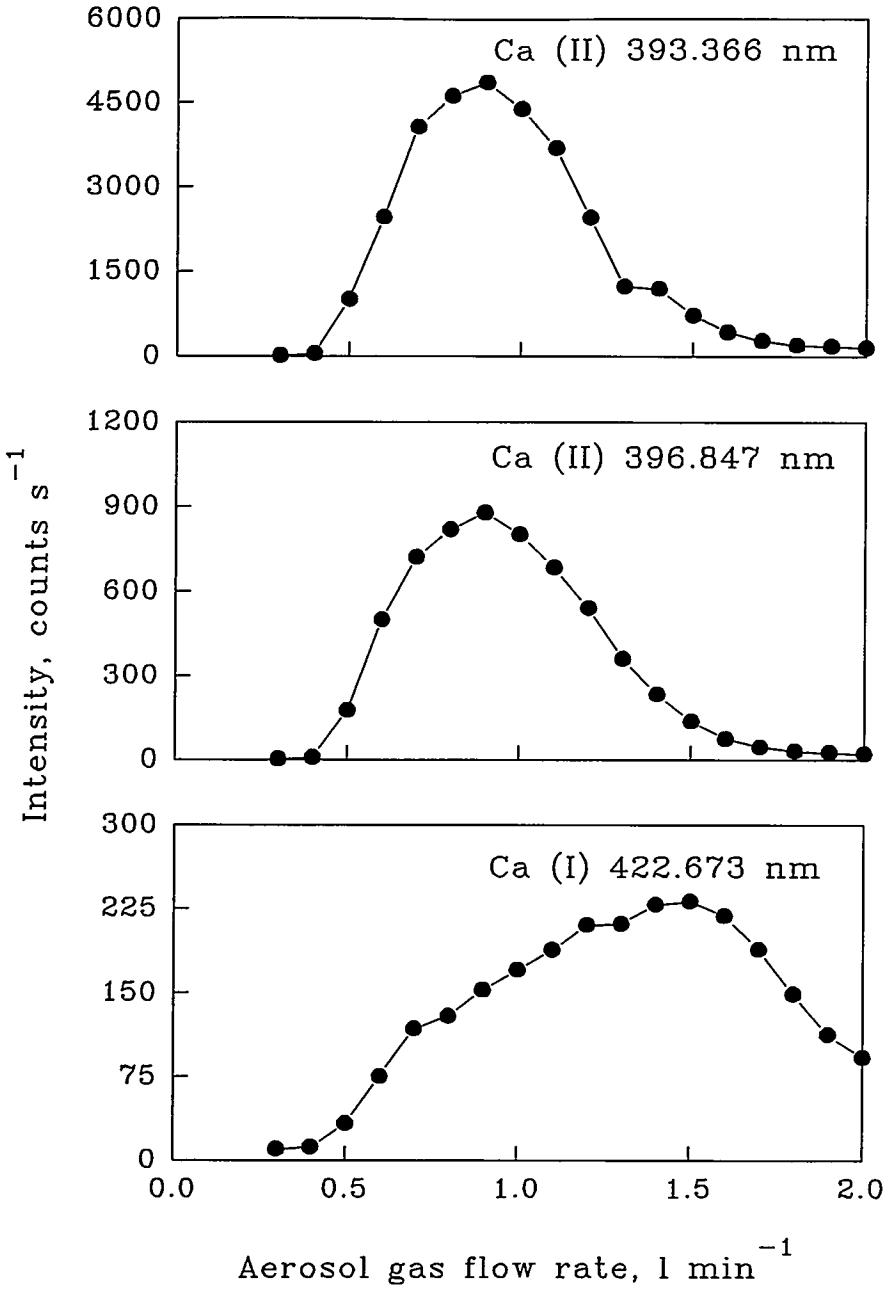

Fig. 8. (continued)

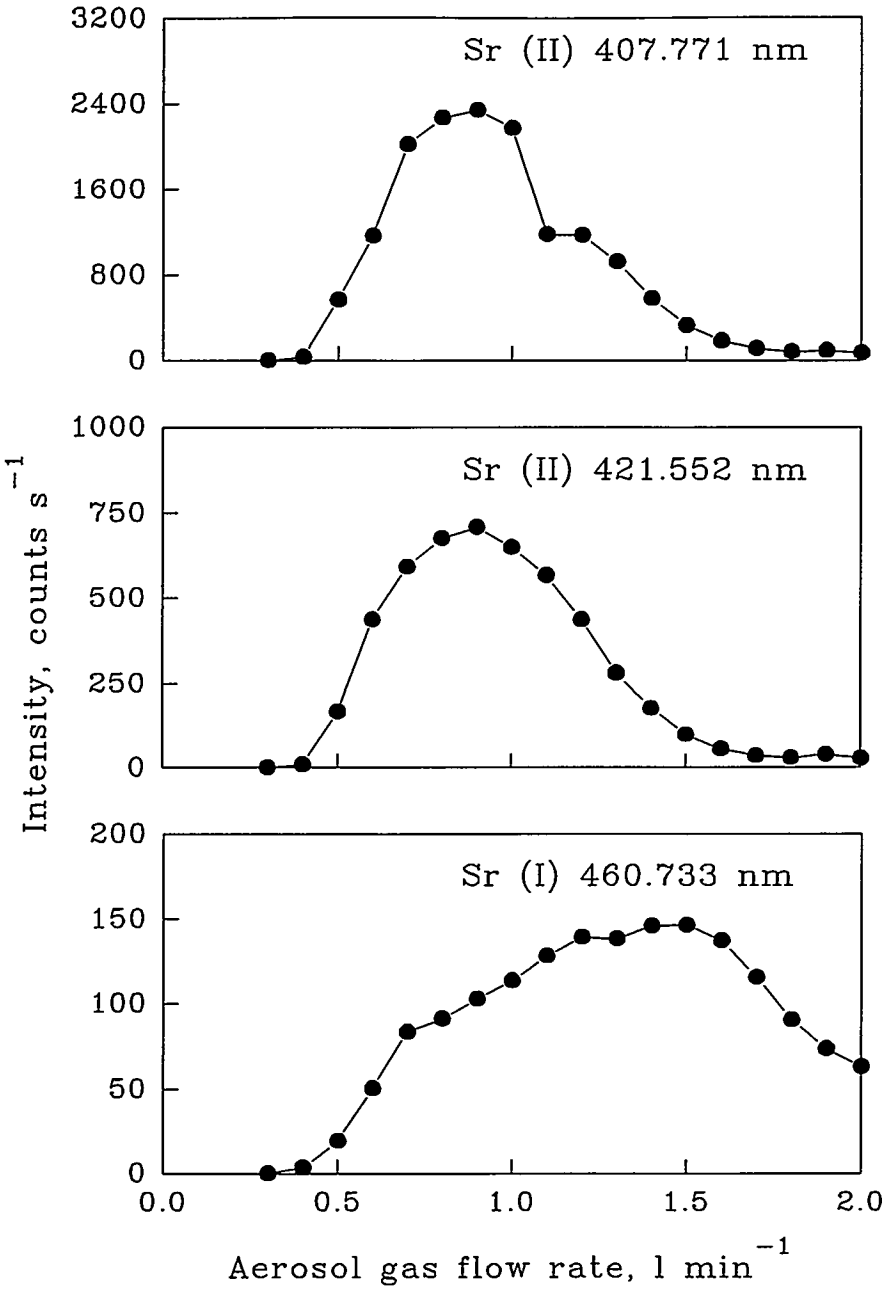

Fig. 8. (continued)

CHAPTER 5. GENERAL CONCLUSIONS

The noise characteristics of aerosols produced by inductively coupled plasma nebulizers were investigated. A laser beam was scattered by aerosol and detected by a photomultiplier tube and the noise amplitude spectrum of the scattered radiation was measured by a spectrum analyzer. The present work illustrates several points of practical interest for analysis by ICP-MS or ICP-AES: (*i*) interference noise in nebulization is at relatively low frequencies (*i.e.*, a few Hz) and is caused by pump fluctuations, not by either the nebulizer or spray chamber; (*ii*) the configuration of and gas flow patterns through the spray chamber can affect levels of 1/f noise and white noise. In particular, the common Scott-type chamber suppresses both 1/f noise and white noise, relative to that in the primary aerosol; (*iii*) the ultrasonic nebulizer suffers from additional 1/f noise beyond that expected from the conical spray chamber usually employed; and (*iv*) the RSD of the scattering signal from the secondary aerosol can be as good as 0.1 %. This value is comparable to the best precision commonly achievable for analytical signals from the ICP in cases where special care is taken to optimize precision. Examples include integrated intensity measurements with a thermostatted spectrometer and Myers-Tracy correction (1) in ICP-AES, or isotope ratio measurements by fast peak hopping in ICP-MS (2). While the sample introduction system can limit precision of spectrochemical measurements with the ICP, this need not always be the case. For example, instabilities associated with the mass bias and mass calibration of the ICP-MS instrument were found to impose limitations upon the precision of isotope ratio measurements (2-4). Further

studies to isolate and characterize each individual source of noise will definitely lead to the better precision of the ICP techniques.

It has been shown in this work that the generalized standard additions method (GSAM) can be applied to an echelle-based polychromator with segmented-array charge-coupled device detectors (SCD), which enables the direct, visual examination of some overlapping spectral lines. The slit translation capability samples a large number of data points (in this case, 56 data points) at fine wavelength intervals within a given spectral window. Therefore, all spectral information available throughout the spectrum can be used to reduce the noise by signal averaging. Pure spectra of each of the components in the sample can be extracted through the GSAM calculation. The validity of the GSAM is confirmed by comparison of the experimental spectrum of the original sample solution with the GSAM reconstructed spectrum. The results are encouraging. Limitations of the GSAM include: (*i*) the need to know the approximate amount of analyte in the sample, so the proper amount of spike can be used, and (*ii*) the time, effort, and potential for contamination associated with multielement spikes. In particular, if overlap between lines of three or more elements is a problem, then more spike additions become necessary, beyond the 6 spikes that suffice in the present work. Evaluation of these potential problems for multielement analysis, particularly for cases in which one of the overlapping lines is much weaker than the other is needed. The present form of the GSAM will not correct for a completely unknown spectral interference. A promising approach for overcoming the limitation of the GSAM is the generalized rank annihilation method (GRAM), which can be used to correct for unexpected spectral

interferences (5-7). For GRAM, a second-order bilinear instrument must be available. The advent of such instrument will no doubt open perspectives for applications of new developments in chemometrics.

In this work, an ICP was extracted into a small quartz vacuum chamber through a sampling orifice in a water-cooled copper plate. Optical emission from the Mach disk region was measured with a new type of echelle spectrometer equipped with two SCD detectors. The spectral background emitted by the Mach disk was very low. Axial profiles of the optical emission of various atom and ion lines were measured. The effects of aerosol gas flow rate on the intensities of various lines were investigated. The relationship between the location of the Mach disk and the pressure in the expansion chamber was also studied. The analyte line intensities were enhanced at higher pressure. Obviously, the analyte signal from the Mach disk must be enhanced further. Several possible ways to implement such enhancements include: (*i*) backfilling the chamber with He, (*ii*) applying RF voltage to an electrode located at a position downstream from the Mach disk, (*iii*) incorporating a magnetic mirror, and (*iv*) simply using an ICP which has higher plasma potential and a stronger secondary discharge (8). Ideally these measures would enhance analyte signal more than background.

References

1. Myers, S. A., and Tracy, D. H., *Spectrochim. Acta, Part B*, 1983, **38**, 1227.

2. Begley, I. S., and Sharp, B. L., *J. Anal. At. Spectrom.*, 1994, **9**, 171.

3. Bley, W. G., *Vacuum*, 1988, **38**, 103.

4. Russ, G. P., and Bazan, J. M., *Spectrochim. Acta, Part B*, 1987, **42**, 49.

5. Sanchez, E., and Kowalski, B. R., *Anal. Chem.*, 1986, **58**, 496.

6. Sanchez, E., and Kowalski, B. R., *J. Chemometrics*, 1988, **2**, 265.

7. Booksh, K. S., and Kowalski, B. R., *Anal. Chem.*, 1994, **66**, 782A.

8. Houk, R. S., Svec, H. J., and Fassel, V. A., *Appl. Spectrosc.*, 1981, **35**, 380.

ACKNOWLEDGEMENTS

During my graduate education at Iowa State University in the past five years, I have had a lot of support and encouragement. There are many people to whom I owe deep appreciation.

First, I would like to express my most sincere gratitude to my major professor, Dr. R. S. Houk, for his guidance and support throughout this work. I appreciate his time on reading several drafts of my papers and his good advice on scientific writing. None of this work could be done without his help. His wide latitude, tolerance, understanding, and support are greatly appreciated.

I would like to thank other members in my committee: Dr. E. S. Yeung, Dr. M. D. Porter, Dr. J. H. Espenson, and Dr. C. S. Oulman. Their critical reading of this manuscript, suggestions, and teachings are greatly appreciated.

Sincere appreciation goes to Dr. Ho-ming Pang who taught me a great deal of scientific instrumentation.

This work was performed at Ames Laboratory under Contract No. W-7405-Eng-82 with the U.S. Department of Energy. The United States government has assigned the DOE Report number IS-T 1733 to this dissertation.

I would like to thank the Department of Chemistry, Iowa State University and the Ames Laboratory, U.S. Department of Energy for providing me with financial support during my graduate study and research.

I would like to thank Royce Winge, David Eckels, Dan Zamzow, Stephan Weeks, Dr. Hai-Chou Chang, Dr. K. A. Gschneidner of the Ames Laboratory, Dr. R. Hendrickson of the Department of Nuclear Engineering, and the Perkin-Elmer Corporation for the loan of various equipments, which made this work possible.

I wish to thank Jerry Hand, Charlie Burg, Steve Lee, and other members of the Ames Laboratory machine shop, Harold Hall of the glassblowing shop of the Department of Chemistry, and L. J. "Oz" Oswood of the Ames Laboratory storeroom. Their talents and experiences helped me a lot.

I would like to thank the former and current members of Dr. Houk's group for their assistance and friendship: Dan Wiederin, Fred Smith, Ke Hu, Sam Shum, Luis Alves, Tonya Bricker, Hongsen Niu, Rocky Warren, Scott Clemons, Xiaoshan Chen, Lloyd Allen, Steve Johnson, Renyi Duan, Mike Minnich, Al Gwizdala, and Narong Praphairaksit. I wish you all the best. I always enjoy your company.

I would like to thank Dr. Z. Ni and Dr. X. Shan of the Research Center for Eco-Environmental Sciences, Chinese Academy of Sciences (advisors for my M.S. degree in analytical chemistry) for leading me into the wonderful field of analytical atomic spectrometry.

I am very grateful to my mother, Yixin Liu, for her love and support throughout my education, and my younger brother, Dr. Yu Luan, for his understanding and taking care of my parents. This dissertation is dedicated to my father, Xianmei Luan, who passed away during the time I was studying here in Ames. My family has always supported me in my endeavors, believed in me, and urged me to do my very best.

Above all, I wish to thank my wife, Xing Yang, for her love, understanding, support, assistance, and encouragement during the course of this work. I thank my parents-in-law, Yongsheng Yang and Meilan Wang, for their generosity. I thank them for giving me such a lovely wife.